

## Tutorial and Review Paper

**Cite this article:** Mishra B, Verma RK, Yashwanth N, Singh RK (2022). A review on microstrip patch antenna parameters of different geometry and bandwidth enhancement techniques. *International Journal of Microwave and Wireless Technologies* **14**, 652–673. <https://doi.org/10.1017/S1759078721001148>

Received: 11 December 2020

Revised: 26 June 2021

Accepted: 29 June 2021

First published online: 3 August 2021

### Key words:



Antenna shape; bandwidth enhancement techniques; electromagnetic tools; circuit theory model; monopole antenna; wearable antenna; multiband antenna

### Author for correspondence:

Brijesh Mishra,

E-mail: [brijesh.mishra0933@gmail.com](mailto:brijesh.mishra0933@gmail.com)

# A review on microstrip patch antenna parameters of different geometry and bandwidth enhancement techniques

Brijesh Mishra<sup>1</sup> , Ramesh Kumar Verma<sup>2</sup>, Yashwanth N<sup>3</sup>   
and Rakesh Kumar Singh<sup>4</sup>

<sup>1</sup>Madan Mohan Malaviya University of Technology, Gorakhpur, UP, 273010, India; <sup>2</sup>Bundelkhand Institute of Engineering & Technology, Jhansi, UP, India; <sup>3</sup>Nagarjuna College of Engineering & Technology, Bangalore, India and <sup>4</sup>Shambhunath Institute of Engineering and Technology, Prayagraj, UP, India

## Abstract

This paper presents a comprehensive review of symmetrically shaped antennas in terms of antenna size, dielectric materials, resonating band, peak gain, radiation pattern, simulating tools, and their applications. In this article, flower shape, leaf shape, tree shape, fan shape, Pi shape, butterfly shape, bat shape, wearable, multiband, monopole, and fractal antennas are discussed. Further, a survey of previously reported bandwidth enhancement techniques of microstrip patch antenna like introduction of thick and lower permittivity substrate, multilayer substrate, parasitic elements, slots and notches, shorting wall, shorting pin, defected ground structure, metamaterial-based split ring resonator structure, fractal geometry, and composite right-hand/left-handed transmission line approach is presented. The physics of these techniques has been discussed in detail which is supported by circuit theory model approach.

## Introduction

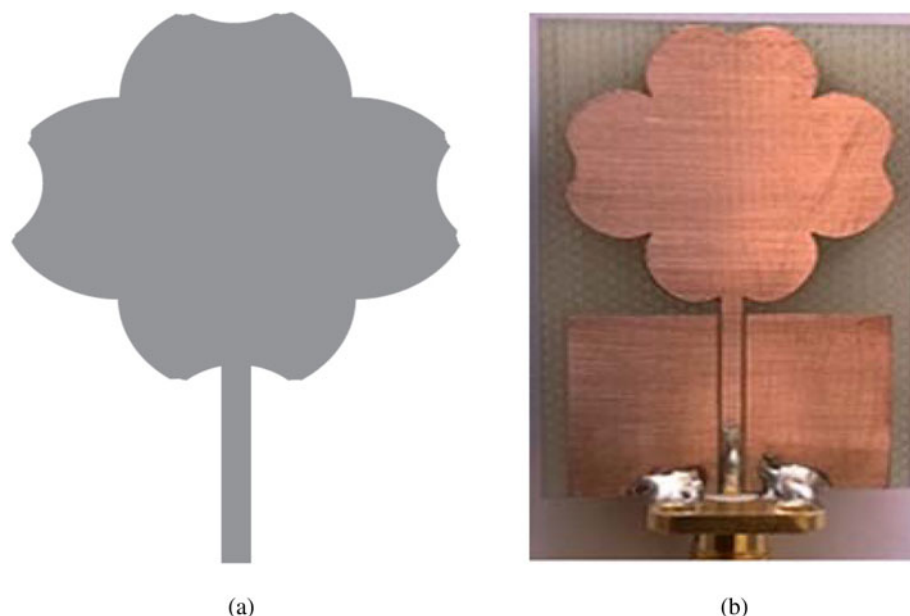
The research on microstrip antennas has taken a leap in the past few decades and is still a surviving and continuously progressing subject because of its low profile, ease in fabrication, and low-cost behavior. Microstrip antenna is one of the most important classes of antenna. The development in various analysis methods and models helps in designing new radiating patches which can be fabricated and tested for use in numerous applications. The numerical techniques such as MoM, FEM, SDT, and FDTD have become more affordable due to advancement in computational power of the computers which has opened new dimensions in performing parametric analysis of the designed antennas [1]. The analytic techniques not only allow the designers to design patch antennas that operate in free space but also extend to meet new specifications for newer applications with new challenges. Microstrip antenna researches were originally driven by the defense sector but now have become increasingly oriented toward telecommunications, automotive, aerospace, and biomedical applications [2]. Satellite and radar communication and wide area communication networks are just a few of communication systems that have benefitted from microstrip antenna design advancements.

With the advancement in technology and great demand for the design of compact planar multiband antennas with simpler geometry for wireless devices [3], the miniaturized and multiband antennas are highly desired. Several techniques for miniaturization are meandering, bending, folding, wrapping, etc. The goal of multiband operation is achieved by ground plane and radiating patch modifications using fixed slots, reconfigurable slots, defected ground and notches, ground strip, etc. [4]. The resonating behavior of microstrip patch antenna can be predicted with the knowledge of physical dimensions of antenna structure. The geometry of the antenna is intuitively conceived and can be designed for specific band of applications.

However, this article is confined to the symmetrical shapes of antenna only and asymmetrical antenna structure is omitted as it will make the paper more voluminous. A simple and general geometry of each type of antenna shape has been considered for discussion. The study of antenna shapes, bandwidth enhancement techniques, and antenna parameters such as resonating band, bandwidth, gain, dimensions, and materials suitable for various applications is presented in the proceeding sections.

## Flower shape antennas

The performance of natural flower-shaped (compare Fig. 1) antennas [5–11] with planar size has been tabulated in Table 1. Most of the flower-shaped antennas of Table 1 are designed using FR4 epoxy substrate whereas antenna reported in [10] is designed using air and copper substrates. The antennas mentioned in [5, 6, 8–10] operate at single resonating band; the



**Fig. 1.** (a) Flower shape antenna geometry. (b) Fabricated photograph of flower shape fabricated antenna; reprint with permission from [5].

antenna mentioned in [11] operates at dual band whereas five-band behavior is observed in rose shape antenna [7] which is having a minimum area of  $144 \text{ mm}^2$  amongst the antennas reported in Table 1. The antenna reported in [11] has the largest planar area ( $8100 \text{ mm}^2$ ). It is interesting to observe that in flower-shaped antennas, the antenna with maximum and minimum planar area exhibits a bandwidth in the vicinity of 500 MHz, which is suggestive of the fact that area of the flower-shaped antennas in case of [7, 11] hardly affects the bandwidth performance of the antenna. However, both the antennas have been designed using different principles; therefore, an exact correlation between size and bandwidth of the two antennas reported in [7, 11] cannot be made.

A maximum simulated peak gain 7.1 dBi and measured peak gain 7.4 dBi are observed in [8, 10], respectively. Flower shape antennas find its applications in the frequency range of 1.03–13.46 GHz. The maximum bandwidth (11 GHz) is observed in the antenna mentioned in [8]. The smallest size ( $12 \times 12 \text{ mm}^2$ ) antenna is reported in [7]. The radiation pattern of flower shape antenna shows almost bidirectional behavior in E-plane and omnidirectional behavior in H-plane.

In column 1 of Table 1, it is observed that the flower shape geometry can be designed after creating distinct small segments on the boundary of radiating patch. This leads to an increase in the overall perimeter ( $P$ ) of the designed radiating patch and finally increases the current length path [5]. The increased current length path generates higher resonance frequencies. Therefore, flower shape antenna is a more suitable candidate for wideband applications as compared to conventional antenna.

### Leaf shape antennas

The overview of leaf shape (compare Fig. 2) antennas [12–17] along with their characteristics and applications has been presented in Table 2. Two antennas [14, 15] have been designed using FR4 epoxy substrate material and are resonating at single band and have same smallest antenna dimension ( $25 \times 16$  and  $20 \times 20 \text{ mm}^2$ ) whereas the antenna reported in [13] has the maximum planar area. The antenna with maximum planar area attains the highest bandwidth of 28.4 GHz and the antennas

with minimum planar areas [14, 15] exhibit bandwidths of 3 and 4 GHz, respectively. In leaf shape antennas, we observe that the large planar area and change in dielectric constant from 4.4 (FR4 epoxy) to 3.5 yield a higher bandwidth of 28.4 GHz.

The ratio of bandwidth of antenna with the largest area [13] to the antenna with minimum area [14] is 7.1:1 whereas the ratio of maximum area to minimum area of the antenna is 16:1. It can be easily inferred that with the increase in antenna area, the bandwidth increases. A simulated and measured gain of 6 and 5.9 dBi, respectively, is reported in [12] and the leaf of rose shape antenna [16]. The radiation pattern of leaf shape antenna shows daunt shape pattern, omnidirectional pattern, asymmetrical and unidirectional pattern, and broadside pattern.








### Tree shape antennas

The performance of natural tree shape (compare Fig. 3) antennas [18–24] is presented in Table 3, which are designed over many different substrates (FR4 epoxy, Teflon, Nylon, and air). Antennas reported in Pythagoras shape antenna [19, 20] are multiband and reconfigurable, respectively, whereas the rest antennas [18, 21–24] are single-band antenna. The antenna reported in [24] has the largest area ( $150 \times 150 \text{ mm}^2$ ) whereas antenna reported in [22] has smaller size among the reported antenna in [18–24]. The antennas mentioned in [21, 22] have smaller patch area and they also yield higher bandwidth of the order of 17.3 GHz [21] and 11.2 GHz [22] whereas antenna [24] yields a very low impedance bandwidth (0.7 GHz) in penalty of large size.

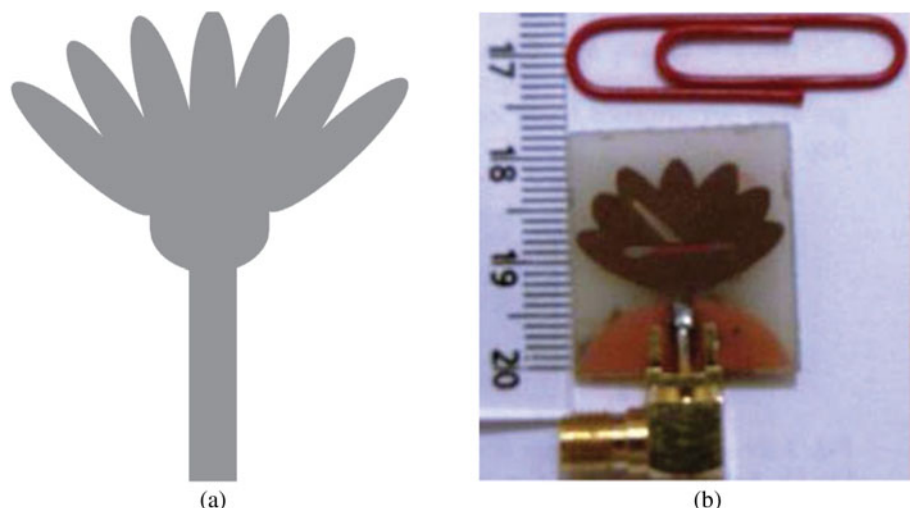
The simulated antenna gains are reported in Table 3 by the authors. The antenna [24] shows the maximum peak gain of 18.4 dBi but it is not suitable for small devices due to its large size. Antenna [22] has a very small area of  $9.2 \times 18.5 \text{ mm}^2$  and can be used in mobile, radio, and satellite applications. The antennas with large planar areas [18, 24] exhibit a smaller fractional bandwidth but exact co-relation cannot be derived as both are fabricated on different substrate materials. The radiation pattern of tree shape antenna shows half-wave dipole-like pattern and omnidirectional pattern.

Owing to the analysis of tree shape antennas, it is observed that most of the antennas [18, 19, 22, 23] in [18–24] come into

**Table 1.** Comparative analysis of flower shape antennas

Shape [Reference]	Antenna size (mm <sup>2</sup> )	Substrate materials	(Resonating band)/bandwidth (GHz) at –10 dB scale	Peak gain (dBi)	Radiation pattern in E-plane/H-plane	Tools used/applications
 Reprint with permission from [5]	28 × 41.8	FR4 epoxy	(2.2–10.6)/8.4 M	5 M	Bidirectional/omnidirectional	HFSS/wireless, microwave imaging system
 Reprint with permission from [6]	34 × 39.1	FR4 epoxy	(2.1–11)/8.9 M	5.03 S	Bidirectional/omnidirectional	HFSS/broadband
 Reprint with permission from [7]	12 × 12	FR4 epoxy	(0.705–1.32)/0.62 M (4.29–4.85)/0.56 M (7.97–8.58)/0.61 M (13.16–13.68)/0.52 M (16.89–17.41)/0.52 M	2.9 S	Bidirectional/Omnidirectional	NR/IEEE802.11/GSM/WLAN/IEEE802.16/Wi-MAX applications
 Reprint with permission from [8]	43 × 51	FR4 epoxy	(2.46–13.46)/11 M	7.1 S	Monopole like/omnidirectional	HFSS/UWB radio systems, military applications
 Reprint with permission from [9]	35 × 38	FR4 epoxy	(2.11–7.84)/5.73 M	5.95 S	Asymmetry/omnidirectional	HFSS/WLAN, WiMAX
 [10]	NR	Air, copper	(3.875–7.45)/3.57 M	7.4 M	NR	IE3D/NR
 [11]	90 × 90	FR4 epoxy	(2.2–2.44)/0.44 S (4–4.5)/0.5 S	1.84 S	NR	HFSS/NR

M, measured result; S, simulated result; NR, not reported; NB, notch band.



**Fig. 2.** (a) Leaf shape antenna geometry. (b) Fabricated photograph of leaf shape antenna; reprint with permission from [15].

the category of fractal antenna. Fractal antenna increases the effective current length path on the radiating surface after filling the blank space with conducting material. Therefore, in wideband applications, tree shape geometry can be replaced with fractal geometry and *vice-versa*.

### Fan shape antennas

Fan shape (compare Fig. 4) antennas [25–31] listed in Table 4 have been designed only for single-band applications. The smallest size antenna has been reported in [28] with maximum measured bandwidth (14.6 GHz) and can be used for ultra-wide band applications. The antenna with the largest planar area of  $125 \times 125 \text{ mm}^2$  is reported in [26] with a very small bandwidth (simulated) of 0.49 GHz.

However, it is difficult to deduce a direct relation between the area and the bandwidth, as only the simulated bandwidth of the antenna with maximum area [26] is reported. A maximum simulated gain of 6 dBi and measured gain of 4.4 dBi is observed in [26, 29] respectively. The radiation pattern of fan shape antenna shows omnidirectional pattern, bidirectional pattern, and dipole-like pattern.

### Pi shape antennas

Table 5 depicts an overview of Pi shape antennas [32–34] (compare Fig. 5). Pi shape antennas [32, 33] show dual resonating behavior while the antenna mentioned in [34] resonates at single frequency. A minimum/maximum measured bandwidth of 0.114/10.7 GHz is observed in [32, 34], respectively. The antenna reported in [32] shows dual- and single-band characteristics with shorting pin and without shorting-pin, respectively. The antenna mentioned in [32] is modified for three band (605, 920, and 1420 MHz) applications and reported in [35]. The resonating band of antenna [35] has changed from dual band to triple band with proper adjustment of feed position.

The antenna mentioned in [32, 33] has smaller size ( $15 \times 15 \text{ mm}^2$ ) and larger size ( $30 \times 40 \text{ mm}^2$ ), respectively, as compared to antennas reported in [32–34]. The operating frequency of Pi shape antenna can alter and makes it suitable for wideband/multiband applications after increasing the current length path. From Table 5, it is concluded that the Pi shape antenna is compact in

size due to its simple structure and suitable for low-frequency applications. Physical resonant length of Pi shape antenna for  $\text{TM}_{10}$  can be approximated as derived in [35].

$$(L_r)_{10} = 2 \left( \frac{L_2}{2} \right) + 2 \left\{ W_1 - \left( \frac{L_2 + W_1 - W_2}{2} \right) \right\} + L_3 + 2 \left( \frac{L_2}{2} \right). \quad (1)$$

We observe a higher impedance bandwidth when RT-Duroid is used as substrate material and a minimum bandwidth when Teflon is used as substrate material. A maximum 6.52 dBi measured peak gain is observed in antenna [32] which is useful in WLAN applications.

### Butterfly shape antennas



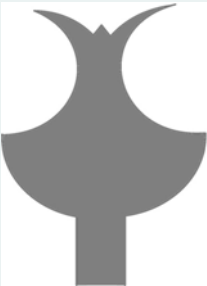


The performance of butterfly-shaped antennas [36–38] is presented in Table 6. The butterfly shape antenna is rarely reported in literature, but the authors searched in literature and found only single-band butterfly shape antenna. A measured bandwidth of 2.21, 6.7, and 1.45 GHz is observed in antennas [36–38], respectively. Operating band of these antennas is varying between 2.6 and 9.3 GHz. Butterfly shape antennas [36, 38] have been designed for low-frequency applications but these are not practically integrable in small devices due to large structure size ( $>27 \times 34 \text{ mm}^2$ ).

Resonance frequency of the butterfly shape antenna can be controlled with the removal of small circles in the left and right arms (compare Fig. 6) of the butterfly shape geometry. Feed position of the butterfly shape antenna can adjust the impedance matching and magnitude of return loss. The antenna mentioned in [38] has a maximum peak gain of 8.8 dBi as compared to the gain reported in the antenna mentioned in [36] (8.3 dBi) and [37] (5 dBi).

### Bat shape antennas


The performance of bat shape antennas [39–41] in terms of size, substrate, resonating band/bandwidth, peak gain radiation pattern, and tools used/applications is presented in Table 7. The geometry of bat shape antenna and fabricated photograph are portrayed in Figs 7(a) and 7(b) respectively. The geometry of bat shape antenna is basically a modified version of ellipse shape geometry. The major

**Table 2.** Comparative analysis of leaf shape antennas

Shape [Reference]	Antenna size (mm <sup>2</sup> )	Substrate materials	(Resonating band)/bandwidth (GHz) at -10 dB scale	Peak gain (dBi)	Radiation pattern in E-plane/H-plane	Tools used/applications
 Reproduced courtesy of The Electromagnetics Academy [12]	30.5 × 35.5	RT/Duroid	(3–14)/11 M (5–6) NB	6 S	Daunt shape/omnidirectional	HFSS, CST/UWB application
 [13]	80 × 80	$\epsilon_r = 3.5$ , $h = 1.5$	(1.3–29.7)/28.4 M	4 M	Monopole-type omnidirectional pattern	CST/L, C, X and Ku band application
 [14]	25 × 16	FR4 epoxy	(9.2–13.2)/4 M	NR	Asymmetrical and unidirectional	HFSS/X-band application
 Reprint with permission from [15]	20 × 20	FR4 epoxy	(4.2–7.2)/3 M Band rejection	3.05 M	Omnidirectional	HFSS/wireless band rejection
 [16]	25 × 25	Air, foam	(4.3–8.3)/4 M	5.9 M	Broadside radiation patterns	HFSS/high speed wireless computer network

(Continued)

Table 2. (Continued.)

Shape [Reference]	Antenna size (mm <sup>2</sup> )	Substrate materials	(Resonating band)/bandwidth (GHz) at -10 dB scale	Peak gain (dBi)	Radiation pattern in E-plane/H-plane	Tools used/applications
 [17]	47.6 × 50	FR4 epoxy	Antenna resonates at 0.54, 3.04 and 3.87 GHz having 51.7, 11.5, and 10.8% simulated impedance bandwidth	NR	Omni-directional for lower frequency and broadside for higher frequency	HFSS/Wi-Fi, WLAN, WiMAX

M, measured result; S, simulated result; NR, not reported; NB, notch band.

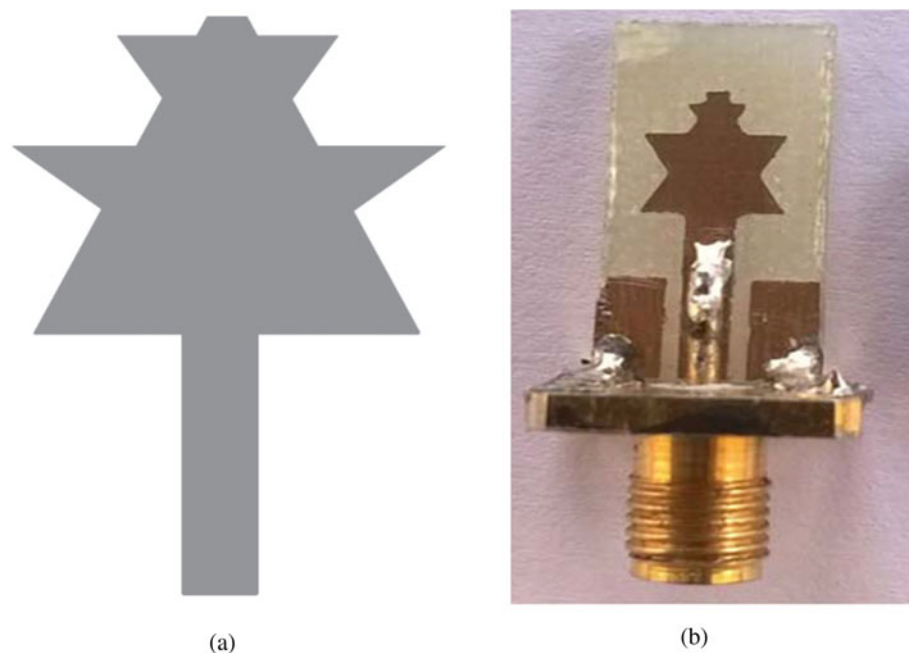


Fig. 3. (a) Tree shape antenna geometry. (b) Fabricated photograph of tree shape antenna; reprint with permission from [22].

axis edge of ellipse shape geometry is notched to design a bat shape antenna. Antennas reported in Table 7 have been designed for single-band operation over FR4 epoxy and RT-Duroid materials, respectively. The bat shape antennas reported in [39–42] exhibit a measured bandwidth of 11.2 GHz [39], 0.26 GHz [40], and 8.73 GHz [41]. A very large bandwidth of 11.2 GHz [39] and a small bandwidth of 0.26 GHz [40] are observed. The antenna mentioned in [39] shows a better absolute bandwidth as compared to the antennas reported in Table 7.

The size of the antenna mentioned in [39] (17 × 27 mm<sup>2</sup>) is also compact as compared to the antennas reported in Table 7. However, the peak gain (9.72 dBi) of antenna [40] has a maximum value as compared to the antennas listed in Table 7. The radiation pattern of the antenna mentioned in [39] shows omnidirectional/quasi omnidirectional and the antenna mentioned in [41] shows monopole-like with bidirectional/omnidirectional, respectively. Bat shape antenna is suitable for WLAN, WiMAX, and UWB applications.

Owing to the bat shape antenna, it is observed that the notches are used on the ellipse-shaped geometry to enlarge the perimeter (*P*) of bat shape antenna which alters the low resonance frequency and finally increases the impedance bandwidth. This argument is validated with the well-known fact that the maximum current distribution appears on the edges rather than the center of the radiating patch.

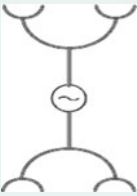





The resonance frequency (*L<sub>f</sub>*) of bat shape, flower shape, leaf shape, and fan shape antenna is given by equation (2) as reported in [39, 41].

$$L_f = \frac{300}{P\sqrt{\epsilon_{eff}}}, \tag{2}$$

where


$$\epsilon_{eff} \approx \frac{\epsilon_r + 1}{2}. \tag{3}$$

**Table 3.** Comparative analysis of tree shape antennas

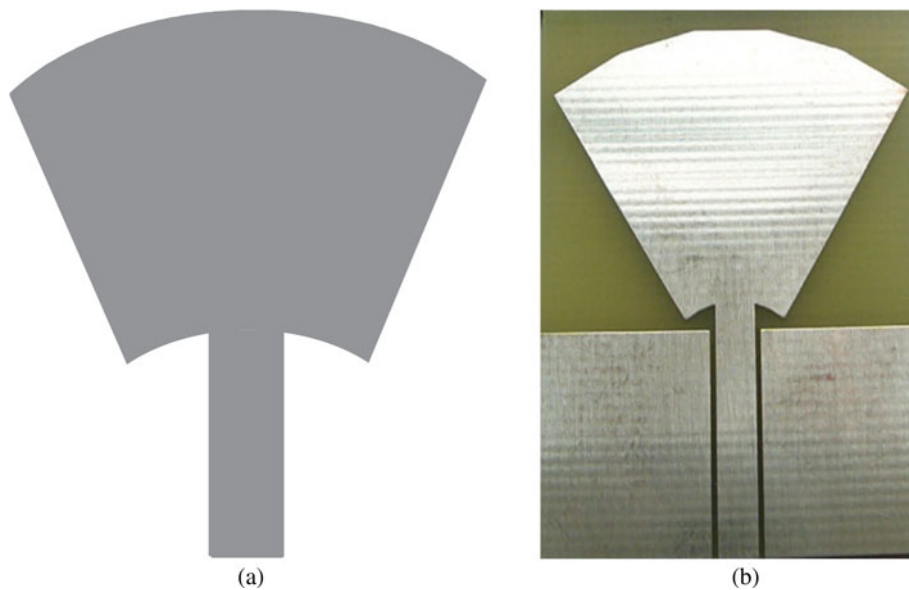
Shape [Reference]	Antenna size (mm <sup>2</sup> )	Substrate materials	(Resonating band)/bandwidth (GHz) at -10 dB scale	Peak gain (dBi)	Radiation pattern in E-plane/H-plane	Tools used/applications
 [18]	50 × 80	FR4 epoxy	(0.92–1.06)/0.14 M	NR	Like half-wave dipole antenna	HFSS/RFID
 [19]	50 × 50	FR4 epoxy	(2.278–2.332)/0.054 S (3.93–4.08)/0.15 S (4.543–4.662)/0.12 S (7.022–7.23)/0.21 S	6.59 S 8.57 S 5.17 S 8.34 S	NR	HFSS/S and C-band applications
 [20]	50 × 60	FR4 epoxy	(1.64–9) M reconfigurable	NR	NR	HFSS/WLAN, WiMAX
 Reprint with permission from [21]	28 × 35	FR4 epoxy	(2.2–19.5)/17.3 M (3.3–3.7)/0.4 NB (5.15–5.85)/0.7 NB	7.5 S	Monopole/omnidirectional	HFSS/WLAN, WiMAX, UWB
 Reprint with permission from [22]	9.2 × 18.5	FR4 epoxy	(4.3–15.5)/11.2 M	4.51 S	Omnidirectional/dipole like pattern	HFSS, CST/mobile, radio, defense, satellite
 Reprint with permission from [23]	20 × 30	FR4 epoxy	(2.8–6.2)/3.4 M	2.7 S	Dipole like radiation pattern	HFSS/MB-OFDM

(Continued)

**Table 3.** (Continued.)

Shape [Reference]	Antenna size (mm <sup>2</sup> )	Substrate materials	(Resonating band)/bandwidth (GHz) at -10 dB scale	Peak gain (dBi)	Radiation pattern in E-plane/H-plane	Tools used/applications
 [24]	150 × 150	Teflon, Nylon, air	(5.5–6.2)/0.7 M	18.4 S	NR	Competitive algorithm/NR

M, measured result; S, simulated result; NR, not reported; NB, notch bands.



**Fig. 4.** (a) Fan shape antenna geometry. (b) Fabricated photograph of Fan shape antenna; reprint with permission from [29].

The resonance frequency of the bat shape antenna can be controlled with alteration in perimeter length ( $P$ ) which is in conformity with equation (2). This argument is not only applicable for bat shape antenna but also used in nature-inspired different types of antenna designs such as flower shape [5, 6], leaf shape [12], fan shape [31], and butterfly shape [38]. These structures also increase the patch periphery without changing the actual patch size which causes the resonance frequency shift toward the lower frequency and *vice-versa*. Moreover, they enhance the antenna bandwidth due to the generation of higher modes by different boundary segments of the patch [5].

### Wearable antennas

The performance of wearable antennas [42–46] with different geometry (compare column 1 of Table 8) has been presented in Table 8. The reported wearable antennas have been fabricated over jeans fabric. The wearable antennas [42, 46] have been

designed for single ultra-wide band applications with a bandwidth of 13.08 and 8.64 GHz, respectively, while the antenna mentioned in [43] has been designed for dual ultra-wide band applications with a bandwidth of 2.29 and 4.23 GHz band. However, the concept of partial ground has been introduced in the antenna mentioned in [43]. The antennas mentioned in [44, 45] show circularly polarized behavior after using defected ground structure (DGS). The antenna mentioned in [44] operates in a single band (bandwidth of 4.2 GHz) whereas the antenna mentioned in [45] operates in triple bands (bandwidth of 0.9, 3.7, and 3.8 GHz).

The size of the antennas mentioned in [45, 46] is same and have smaller planer area ( $25 \times 25 \text{ mm}^2$ ) as compared to the antennas reported in Table 8. A minimum peak gain of 3.8 dBi of the antenna mentioned in [42] and a maximum peak gain of 5.7 dBi of the antenna mentioned in [43] have been reported. Omnidirectional radiation pattern behavior of the antennas reported in [42, 43, 45, 46] and bidirectional/omnidirectional radiation pattern of the antenna reported in [44] in E-plane/H-plane are observed. Wearable antennas reported in Table 8



**Table 4.** Comparative analysis of fan shape antennas

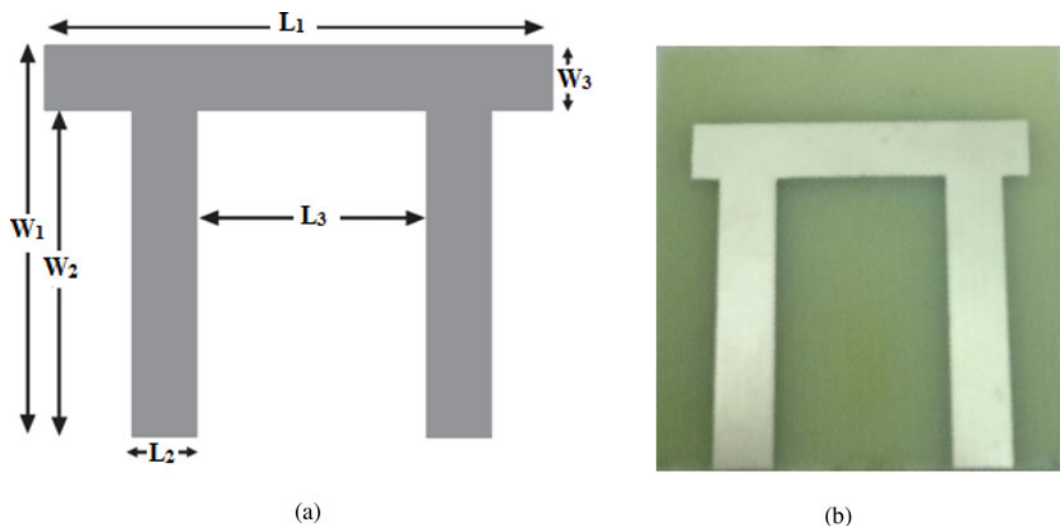
Ref.	Antenna size (mm <sup>2</sup> )	Substrate materials	(Resonating band)/bandwidth (GHz) at -10 dB scale	Peak gain (dBi)	Radiation pattern in E-plane/H-plane	Tools used/applications
[25]	50 × 50	FR4 epoxy	(1.976–2.056)/0.08 M (2.000–2.060)/0.06 M	1.4 M 1.04 M	NR	HFSS/mobile communication
[26]	125 × 125	RT/Duroid, FR4 epoxy, foam	(1.12–1.61)/0.49 S	6 S	NR	NR/L-band GPS satellite communication
[27]	36.5 × 20	$h=0.5$ mm, $\epsilon_r=2.65$	(3.1–10.6)/7.5 S Three notch bands	NR	Omnidirectional	HFSS/UWB suppression with WiMAX, WLAN RFID
[28]	12 × 18	FR4 epoxy	(2.8–17.4)/14.6 M, (5–6) NB, (7.25–7.75) NB, (8.02–8.4) NB	NR	Bidirectional pattern/ omnidirectional	HFSS/UWB
[29]	30 × 35	FR4 epoxy	(3.1–10.6)/7.5 M	4.4 M	Omnidirectional/dipole	HFSS/UWB applications
[30]	20 × 37.6	$\epsilon_r=2.65$ $h=0.4$ mm $\tan\delta=0.001$	(3–10.8)/7.8 M	NR	Dipole/omni-directional	CST/UWB radio
[31]	50 × 50	FR4 epoxy	(1.780–1.817)/0.037 M	1.5 M	RHCP is its co-polarization LHCP is its cross-polarization	CST/GSM applications

M, measured result; S, simulated result; NR, not reported; NB, notch bands.

**Table 5.** Comparative analysis of Pi shape antennas

Ref.	Antenna size (mm <sup>2</sup> )	Substrate materials	(Resonating band)/bandwidth (GHz) at -10 dB scale	Peak gain (dBi)	Radiation pattern in E-plane/H-plane	Tools used/applications
[32]	15 × 15	Teflon	(5.147–5.358)/0.211 M (5.712–5.826)/0.114 M	6.52 M	NR	Microwave studio/ WLAN
[33]	30 × 40	FR4 epoxy	(1.48–1.68)/1.52 M (1.87–1.88)/1.81 M	1.2 M 3 M	Broadside radiation	IE3D/NR
[34]	22.8 × 26.6	RT/Duroid	(1.08–11.8)/10.7 M (5.07–5.84) NB	NR	NR	HFSS/UWB applications

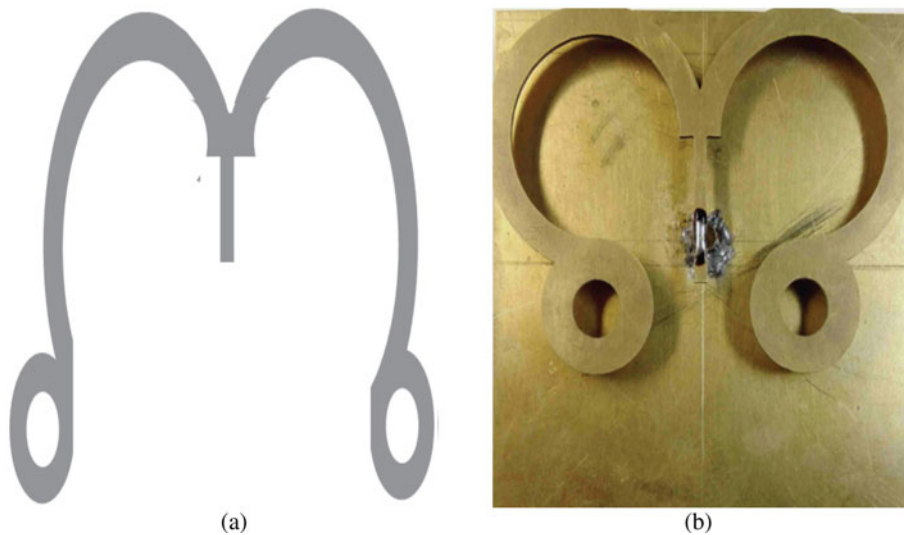
M, measured result; S, simulated result; NR, not reported; NB, notch bands.

**Fig. 5.** (a) Pi shape antenna geometry. (b) Fabricated photograph of Pi shape antenna.

**Table 6.** Comparative analysis of butterfly shape antennas

Ref.	Antenna size (mm <sup>2</sup> )	Substrate materials	(Resonating band)/bandwidth (GHz) at -10 dB scale	Peak gain (dBi)	Radiation pattern in E-plane/H-plane	Tools used/applications
[36]	80 × 80	Metal, air	(4.15–6.36)/2.21 M	8.3 M	NR	HFSS/RFID, wireless
[37]	300 × 300	PEC material	(2.6–9.3)/6.7 M	5 M	NR	Zeland software/radar, wireless
[38]	27 × 34	RT/Duroid 5880	(6.02–7.47)/1.45 M	8.8 M	Broadside	CST/C-band

M, measured result; S, simulated result; NR, not reported; NB, notch bands.



**Fig. 6.** (a) Butterfly shape antenna geometry. (b) Fabricated photograph of butterfly shape antenna; reprint with permission from [36].

find the applications in biomedical, sensors, WiMAX, WLAN, C/ X/Ku, and UWB bands.

The designing procedure of wearable antenna is almost same as the patch antenna. However, wearable antenna uses the flexible substrates for antenna design due to its practical implantation on human body. After examining the wearable antennas reported in Table 8, it is concluded that the wearable antenna plays a very vital role in medical applications but following issues are yet to be improved: to reduce the bending effect, make it washable, reduce electromagnetic interference in human body.

### Multiband antennas

The performance of multiband antennas [47–53] up to seven resonating bands has been presented in Table 9. The multiband antennas with simple design are highly desired for wireless applications as it is integrated into smart devices for multiple applications with the use of single antenna. The design of multiband antenna has been achieved in Table 9 after modification on radiating patch and ground plane structure using slots, notches, and defected ground, etc. [51]. The multiband antennas [47, 48] have been designed for dual (bandwidth of 0.4 and 2.2 GHz) and triple bands (bandwidth of 0.05, 0.21, and 0.43 GHz), respectively, while the antennas mentioned in [49] and [50] have been designed for quad band applications with a bandwidth of 0.32, 0.09, 0.09, 0.04 GHz and 0.25, 0.31, 0.3, 1.04 GHz, respectively. The penta-band antenna [51] resonates in 3.54–9.78 GHz with a maximum bandwidth of 0.38 GHz, hexa-band antenna [52]

resonates in 11.20–23.55 GHz with a maximum bandwidth of 1.77 GHz, and hepta-band antenna [53] resonates in 1.57–7.91 GHz with a maximum bandwidth of 0.52 GHz. The antennas mentioned in [47, 49–51] have been designed with partial ground structure and the antennas mentioned in [48, 52] have been designed with the introduction of slots and notches on the radiating patch for multiband operations whereas hepta-band antenna [53] has been designed using multiple substrate layers with photonic bandgap (PBG) structure to achieve seven band resonances.

The antennas [47–53] reported in Table 9 have been fabricated over FR4 epoxy substrate. The antenna mentioned in [47] has smaller planar area (15 × 20 mm<sup>2</sup>) and the antennas mentioned in [48, 53] have larger planar area (39 × 47.6 mm<sup>2</sup>) as compared to the antennas reported in Table 9. A minimum peak gain of 1.2 dBi of the antenna mentioned in [51] and a maximum peak gain of 8 dBi of the antenna mentioned in [49] have been reported. Omnidirectional radiation pattern behavior of the antenna mentioned in [49], bidirectional/omnidirectional radiation pattern of the antennas mentioned in [47, 48, 50], dipole-like/omnidirectional radiation pattern of the antenna mentioned in [51], and directional radiation pattern behavior of the antenna mentioned in [52] in E-plane/H-plane are observed.

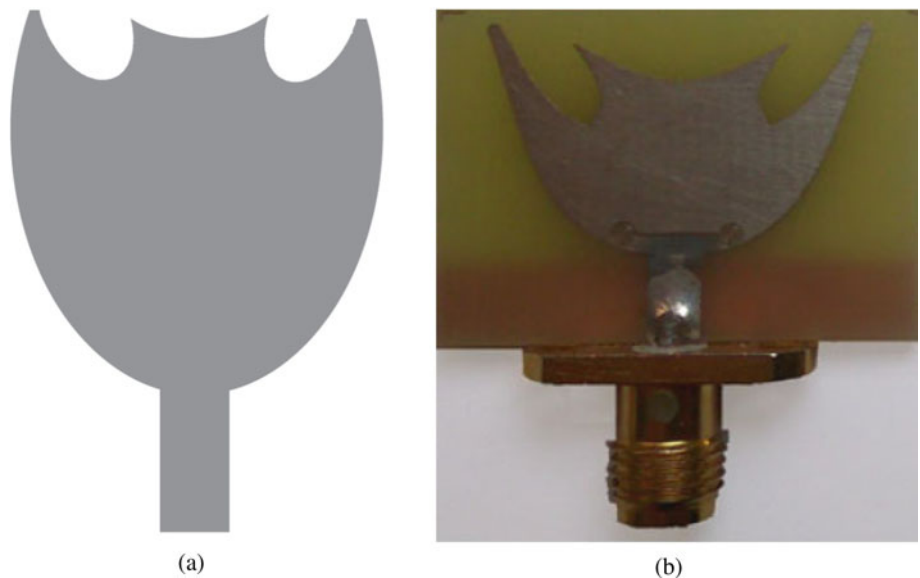
### Monopole antennas

In Table 10, the performances of monopole antennas [13, 15, 17, 29, 37, 38] are presented. The monopole antennas with leaf shape

**Table 7.** Comparative analysis of bat shape antennas

Ref.	Antenna size (mm <sup>2</sup> )	Substrate materials	(Resonating band)/bandwidth (GHz) at -10 dB scale	Peak gain (dBi)	Radiation pattern in E-plane/H-plane	Tools used/applications
[39]	17 × 27	FR4 epoxy	(2.75–13.98)/11.2 M (3.21–4.02) NB, (4.99–6) NB	4.1 M	Omnidirectional/quasi omnidirectional	HFSS/WLAN, WiMAX
[40]	35 × 19	RT/Duroid	(14.64–14.90)/0.26 M	9.72 M	NR	Sonnet suites/NR
[41]	27 × 19	FR4 epoxy	(2.83–11.56)/8.73 M (3.3–4.2) NB (4.9–6) NB	4.5 M	Monopole-like with bidirectional/omnidirectional	HFSS/CST

M, measured result; S, simulated result; NR, not reported; NB, notch bands.



**Fig. 7.** (a) Bat shape antenna geometry. (b) Fabricated photograph of bat shape antenna; reprint with permission from [41].

geometry have been reported in [13, 15, 17]. A measured bandwidth of 28.4 and 3 GHz of antennas reported in [13, 15] is, respectively, observed. Triple band antenna [17] yields the impedance bandwidth of 51.7, 11.5, and 10.8% at frequencies 0.54, 3.04, and 3.87 GHz, respectively. A fan shape monopole antenna reported in [29] resonates in 3.1–10.6 GHz band and yields a bandwidth of 7.5 GHz. Monopole antennas with butterfly shape [37] and bat shape [38] resonate in single band with a bandwidth of 7.5 and 11.2 GHz, respectively.

A measured maximum/minimum bandwidth of 28.4/3 GHz is observed in [13, 15], respectively. However, the antenna mentioned in [17] reported only simulated bandwidth wherein a maximum/minimum bandwidth of 51.7/10.8% is observed. The antenna mentioned in [15] has smaller planar area (20 × 20 mm<sup>2</sup>) and the antenna mentioned in [37] has the largest planar area (300 × 300 mm<sup>2</sup>) compared to the antennas reported in Table 10. However, the antenna mentioned in [15] has smaller bandwidth among the antennas listed in Table 10. The bandwidth of the antenna mentioned in [13] is larger but the size (80 × 80 mm<sup>2</sup>) of the antenna is significantly large.






A minimum/maximum peak gain of 3.05/5 dBi is observed in [15, 37], respectively. A maximum peak gain of 5 dBi is offered in the antenna mentioned in [37] but practically not suitable for small devices due to its large antenna size. Radiation pattern of the monopole antennas is almost omnidirectional in nature.

### A brief survey on bandwidth enhancement techniques

There are several bandwidth enhancement techniques such as introduction of thick and lower permittivity substrate, multilayer substrate, parasitic elements, slots and notches, shorting wall, shorting pin, DGS, metamaterial-based split ring resonator (SRR) structure, fractal geometry, and composite right-hand/left-hand transmission line (CRLH-TL) approach that have been tabulated in Table 11. Thick and low permittivity substrate antenna is reported here for wideband applications (35% bandwidth) [54]. Stacked microstrip patch antennas [55–59] consist of different layers of dielectric material along with patch and parasitic patch that are electronically coupled to the feed line. The stack antenna increases the overall height and back radiation of the MSAs which is not desirable for conformal applications. However, stacked broadband MSAs improve the gain of the antenna with negligible degradation in radiation pattern over the entire bandwidth as compared to the single-layer antenna.

Gap coupled microstrip patch antenna is the most popular technique in practice that is used to enhance the bandwidth where two patches are separated by a suitable gap length. In this, one patch is directly excited by feed (fed patch) and other is radiated by fed patch (parasitic patch) [60–62]. Electronically coupled (stacked antenna), aperture coupled, and gap coupled antenna are known as multi resonating antennas that yield broad bandwidth but their large size and volume make them

**Table 8.** Comparative analysis of wearable antennas

Shape [Reference]	Antenna size (mm <sup>2</sup> )	Substrate materials	(Resonating band)/bandwidth (GHz) at -10 dB scale	Peak gain (dBi)	Radiation pattern in E-plane/H-plane	Tools used/applications
 Reprint with permission from [42]	60 × 60	Jeans fabric	(8.87–21.95)/13.08 S	3.8 S	Overall omnidirectional	CST/WiMAX
 [43]	40 × 40	Jeans fabric	(3.01–5.3)/2.29 M (8.12–12.35)/4.23 M	5.7 S	Overall omnidirectional	CST/WiMAX/ WLAN/X-band
 [44]	43.5 × 42	Jeans fabric	(4.8–9)/4.2 M	5.19 M	Bidirectional/ omnidirectional	CST/WLAN/ HIPER LAN/2/ C-band
 [45]	25 × 25	Jeans fabric	(3.4–4.3)/0.9 M (4.7–8.4)/3.7 M (10.3–14.1)/3.8 M	4.85 M	Overall omni-directional pattern	CST/WLAN, C-band and X/ Ku-band
 [46]	25 × 25	Jeans fabric	(2.96–11.6)/8.64 M	5.47 M	Quasi-omnidirectional/ omnidirectional patterns	CST/UWB

M, measured result; S, simulated result; NR, not reported; NB, notch bands.

unsuitable for the antenna array element [1]. A maximum of 44.9% bandwidth is achieved in stacked antennas [56] and up to 30% improved bandwidth is reported by [62] in all gap coupled antennas. Dual (14.08/13.32%) and wideband (25.09%) multilayer antenna with improved gain for WLAN/WiMAX applications is reported [55].

The shorting wall and shorting pin loaded antennas [63–71] have been reported in Table 11. A maximum bandwidth (98.22%) is achieved by using a folded patch and shorting pin

techniques [65] where a shorting copper pin is used to connect the upper patch and ground plane. Antenna layer shorted by a conducting wall or folded wall to achieve the broad bandwidth up to 28.1% impedance bandwidth is reported by Li *et al.* [68]. The slot on the radiating patch creates another resonance in addition to the patch resonance thereby increasing the bandwidth at the expense of increasing back radiation but it suffers from poor gain and degradation of radiation pattern [1, 72, 73, 74]. Introduction of slot on the patches has led to an impedance

**Table 9.** Comparative analysis of multiband antennas

Ref.	Antenna size (mm <sup>2</sup> )	Substrate materials	(Resonating band)/bandwidth (GHz) at -10 dB scale	Peak gain (dBi)	Radiation pattern in E-plane/H-plane	Tools used/applications
[47]	15 × 20	FR4 epoxy	(2.8–3.2)/0.4 M (4.0–6.2)/2.2 M	2 S	Bidirectional/omnidirectional radiation pattern	CST/S-band, WiMAX and Wi-Fi bands
[48]	39 × 47.6	FR4 epoxy	(1.30–1.35)/0.05 M (1.94–2.15)/0.21 M (2.46–2.89)/0.43 M	3.29 S 3.08 S 3.48 S	Bidirectional/omnidirectional radiation pattern	IE3D/L-band and Bluetooth applications
[49]	25 × 25	FR4 epoxy	(3.25–3.57)/0.32 M (4.20–4.29)/0.09 M (5.41–5.50)/0.09 M (5.73–5.77)/0.04 M	8 S	Nearly omnidirectional radiation pattern	HFSS/WLAN and WiMAX applications
[50]	24 × 16.4	FR4 epoxy	(1.64–1.89)/0.25 M (2.39–2.70)/0.31 M (3.40–3.70)/0.30 M (5.15–6.19) /1.04 M	1.7 S 1.8 S 2.61 S 2.86 S	Bidirectional and omnidirectional radiation pattern	Keysight ADS/WiMAX, WLAN and GSM applications
[51]	32 × 32	FR4 epoxy	(3.54–3.61)/0.07 M (5.88–6.09)/0.19 M (6.68–6.80)/0.12 M (8.36–8.74)/0.38 M (9.40–9.78)/0.38 M	1.2 M 1.6 M 2.1 M 2.5 M 2.7 M	Dipole-like and almost omnidirectional-like pattern	HFSS/WLAN, WiMAX, Satellite TV and X-band
[52]	30 × 30	FR4 epoxy	(11.20–11.99)/0.79 M (13.45–15.22)/1.77 M (16.87–17.70)/0.83 M (19.01–20.19)/1.18 M (20.77–21.53)/0.76 M (22.17–23.55)/1.38 M	7.39 S 2.25 S 6.65 S 5.83 S 6.02 S 7.31 S	Directional radiation pattern	HFSS/X, Ku and K
[53]	39 × 47.6	FR4 epoxy	(1.57–1.70)/0.13 M (2.18–2.45)/0.27 M (3.70–3.90)/0.20 M (4.64–5.11)/0.47 M (5.51–5.66)/0.15 M (6.18–6.70)/0.52 M (7.78–7.91)/0.13 M	7.16 S 5.08 S 4.53 S 6.32 S 4.55 S 4.74 S 6.04 S	NR	IE3D/L, S and C-band applications

M, measured result; S, simulated result; NR, not reported; NB, notch bands.

( $Z_s = R_r + jX_c$ ) parallel to the input impedance of the antenna. The slot impedance consists of radiation resistance ( $R_r$ ) and the reactive component ( $X_c$ ) in series that alters the total input impedance of the patch antenna [75]. Enhanced bandwidth up to 25.09% [55] and 48.8% [73] is achieved in slot loaded antenna.

Researchers are also trying to enhance the antenna gain and they have already proposed several gain enhancement techniques in last decades such as addition of dielectric substrates over the primary dielectric substrate [76, 77], up to 4 dBi increased gain is obtained using metamaterial structure [78]; PBG structure is also used to increase significant gain [79], electromagnetic band gap structure has been used to achieve up to 2.9 dBi enhanced gain [80] and slotted ground plane structure is reported to enhance the antenna gain up to 3.3 dBi [81].

To design high efficiency antenna, impedance of fed network and radiating patch impedance should be conjugated to match perfectly. To overcome the poor radiation efficiency problem of MSA, a dual feed circularly polarized antenna is chosen to improve radiation efficiency [82].

Small planar size of antenna is in more demand in advanced communication technology due to their compatibility with monolithic microwave integrated circuit and array antenna elements. Several methods have been developed to reduce the antenna structure size such as low-temperature co-fired ceramic technology

with only  $8 \times 8 \times 1.1 \text{ mm}^3$  of antenna volume is reported [83], an effective approach of inductively loading the patch using a cuboid ridge is presented [84], and a square patch antenna with loading of slits and truncated corners is reported while 36% antenna size is reduced as compared to conventional square patch antenna [85].

Owing to the above study, it is observed that many techniques have been reported in literature to improve the antenna parameters such as bandwidth, gain, and radiation efficiency. In this section, only bandwidth enhancement techniques have been carried out and the techniques for gain and radiation efficiency improvement are omitted as it makes this work more voluminous.

### Effects of thick substrate, stacked substrate, and parasitic substrate

The thick substrate (S. No. 1 in Table 11) provides high gain and large bandwidth of microstrip patch antenna but at the same time it makes antenna more voluminous and limits the applications of microstrip patch antenna. The alteration in substrate height (h) shifts the resonating frequency toward lower band (with increase in substrate height) or toward higher frequency band (with decrease in substrate height)

**Table 10.** Comparative analysis of monopole antennas

Ref.	Antenna size (mm <sup>2</sup> )	Substrate materials	(Resonating band)/bandwidth (GHz) at -10 dB scale	Peak gain (dBi)	Radiation pattern in E-plane/H-plane	Tools used/applications
[13]	80 × 80	$\epsilon_r = 3.5$ , $h = 1.5$	(1.3–29.7)/28.4 M	4 M	Monopole-type omnidirectional pattern	CST/L, C, X, Ku band application
[15]	20 × 20	FR4 epoxy	(4.2–7.2)/3 M Band rejection	3.05 M	Omnidirectional	HFSS/wireless band rejection
[17]	47.6 × 50	FR4 epoxy	Antenna resonates at 0.54, 3.04, and 3.87 GHz and having 51.7, 11.5, and 10.8% simulated impedance bandwidth	NR	Omni-directional for lower frequency and broadside for higher frequency	HFSS/Wi-Fi, WLAN, WiMAX
[29]	30 × 35	FR4 epoxy	(3.1–10.6)/7.5 M	4.4 M	Omnidirectional/dipole	HFSS/UWB applications
[37]	300 × 300	PEC material	(2.6–9.3)/6.7 M	5 M	NR	Zeland/radar, wireless
[38]	17 × 27	FR4 epoxy	(2.75–13.98)/11.2 M (3.21–4.02) NB, (4.99–6) NB	4.1 M	Omnidirectional/quasi omnidirectional	HFSS/WLAN, WiMAX

M, measured result; S, simulated result; NR, not reported; NB, notch bands.

[86] which is also in conformity with equation (4).

$$h = \frac{0.3c}{2f\pi\sqrt{\epsilon_r}}, \quad (4)$$

where  $c$  is speed of light,  $f$  is resonating frequency,  $\epsilon_r$  is relative permittivity of dielectric.

The simplified circuit diagram of thick substrate microstrip patch antenna is like rectangular microstrip patch antenna as presented at S. No. 1 in Table 11. The value of electrical circuit elements can be calculated with the analysis presented in [87–89]. After relating equation (4) and the analysis presented in [87–89], it may be concluded that there is a decrease in capacitive effect, quality factor, and resonating frequency of microstrip patch antenna whereas the inductive effect increases with the increase in substrate height. However, authors have reported thin substrate microstrip antenna for improved bandwidth (30%) with a penalty of spurious radiation and poor gain [90].

In designing microstrip patch antenna, the use of thick substrate (S. No. 1 in Table 11) results in high gain and large bandwidth but at the same time it limits its applications by making it more voluminous.

The multilayer structure consists of two or more substrate layers with different dielectric constants (S. No. 2 in Table 11) to increase the bandwidth and gain of the antenna. The stacked antenna shows a small degradation in radiation pattern over entire bandwidth as compared to the conventional antenna. The drawback of stacked antenna is that it increases the antenna volume and generates spurious radiation in aperture-coupled stacked antenna which restricts antenna applications in small devices. The effect of multilayer structure in terms of effective dielectric constant, resonating frequency, mutual inductance, and capacitance of stacked and parasitic patches are discussed in reported works [4, 40, 91].

The gap-coupled structure (S. No. 3 in Table 11) of strip conductor is represented by an equivalent T or  $\pi$  network [62]. The plate capacitance ( $C_p$ ) is introduced because of field distribution at the edge of the conductor whereas gap capacitance ( $C_g$ ) arises

due to the coupling effect of two conductors. Large air gap between two patches may be ineffective and behave as single patch antenna due to weak electric field at the edges of conductors. The resonant frequency decreases exponentially with an increase in gap length due to the significant shift in zero reactance point of the antenna. The gap between patches introduces gap capacitance ( $C_g$ ) and plate capacitance ( $C_p$ ) as illustrated at S. No. 3 in Table 11 and values can be referred from antennas reported in [62, 87, 92–94].

### Effects of shorting pin and shorting wall

A copper rod is generally used to short the radiating path and ground via dielectric substrate (compare S. No. 4 in Table 11). The copper rod comprises of an inductance ( $L_{sh}$ ) in parallel to the patch antenna circuit that is illustrated at S. No. 4 in Table 11. The inductive effect of shorting copper rod is formulated in equation (5) as stated in [92, 93].

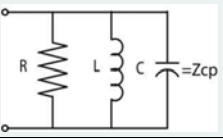
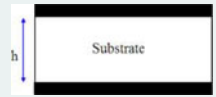
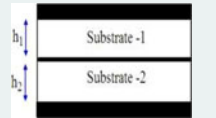
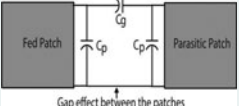

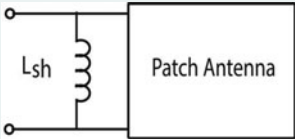
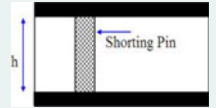
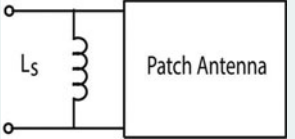
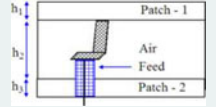


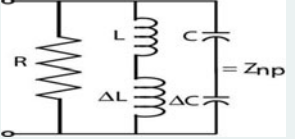

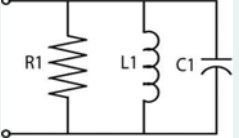

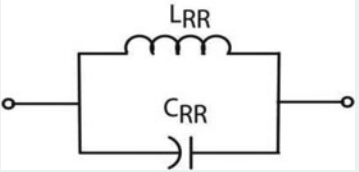


$$L_{sh} = \frac{\eta_0 W_p L_p}{2\pi c} \ln \left[ \frac{4c}{AW_p D \sqrt{\epsilon_r}} \right], \quad (5)$$

where  $A =$  Euler's constant = 0.5772,  $D$  is diameter of the shorting pin, and  $\eta_0 = 120\pi$ .

The shorting wall or metal plate is used to short the two regions (radiating patch and ground patch) of microstrip patch antenna (compare S. No. 5 in Table 11) to overcome the surface wave effects. An introduction of shorting pin between radiation patch and ground plane leads to control the operating transverse magnetic (TM) modes, antenna gain, resonance size, and bandwidth due to the significant change in current length path on the radiating surface [74]. Introduction of shorting wall results in wideband behavior of microstrip patch antenna. Also, parallel inductive load is introduced due to shorting wall which can be calculated as [95]:

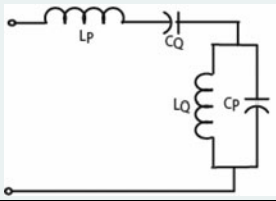

$$L_s = 0.2h \left[ \log \frac{2h}{l+t} + 0.2235 \frac{l+t}{h} + 0.5 \right], \quad (6)$$

**Table 11.** Comparative overview of bandwidth enhancement techniques of MSAs

S. No.	Equivalent circuit	Techniques	(-10 dB bandwidth (%) [Reference])	Antenna structure
1		Thick and low permittivity substrate	(35) [54]	
2	The equivalent circuit of stacked antenna is not fixed. However, it can be predicted with structures used on different layers	Stacking substrate	(14.08/13.32) [55], (38.41/44.9) [56], (19.3/18.6) [57], (3.42/4.83) [58], (1/3.1) [59]	
3		Parasitic elements	(15.4/25.8) [60], (16.5) [61], (30) [62]	
4		Shorting pin	(8) [63], (10) [64], (94.17/98.22) [65], (7.7/13.7) [66], (90) [67]	
5		Shorting wall	(28.1) [68], (28) [69], (8/8) [70], (70) [71]	
6		Loading of slot	(25.09) [55], (48.7) [72], (48.8) [73], (5.4) [75], (4.13/8.82) [88]	
7		Loading of notch	(4.29/8.59) [89], (9.94/12.99) [96], (1.51/4.29) [97], (27.89) [98], (13.2) [99]	
8		Defected ground structure (DGS)	(112.4) [100], (54.65) [2], (22) [101]	
9		Split ring resonator (SRR)	(12) [103], (6.6/4.8) [104], (11.4) [105], (17.66) [106]	
10	The equivalent circuit of fractal antenna is not fixed. However, it can be predicted with the knowledge of fractal geometry	Fractal geometry	(Max. 61.38) [7], (113.13) [22], (75.5) [23], (Max. 3.3) [108], (30.17) [109], (Max. 13.2) [110], (13.3) [111] (83.13) [112]	

(Continued)

Table 11. (Continued.)

S. No.	Equivalent circuit	Techniques	(-10 dB bandwidth (%)) [Reference]	Antenna structure
11		Composite right/left-handed transmission line (CRLH-TL) approach	(160) [113], (max. 170) [114], (max. 14.1) [115], (more than 100 MHz) [116], (max. 2200 MHz) [117], (max. 100 MHz) [118]	

where,  $l$  = length of shorting wall,  $t$  = width of shorting wall,  $h$  = height of substrate.

**Effects of slot and notch analysis of notch loaded patch**

The introduction of a notch ( $L_n \times W_n$ ) on the patch (compare S. No. 7 in Table 11) creates multiple resonance and directs current flow in two different ways, normal to the patch and around the notches. Current length normal to patch is responsible for resonance at the designed frequency of the initial patch ( $L_p \times W_p$ ) whereas current length around the notches generates second resonance frequency. Due to this phenomenon, the inductance and capacitance of equivalent circuit of antenna get replaced with a series inductance ( $\Delta L$ ) and a series capacitance  $\Delta C$  respectively which can be calculated as [88].

$$\Delta L = \frac{h\mu_0\pi}{8}(L_n/W_n)^2, \tag{7}$$

$$\Delta C = \left(\frac{L_n}{W_n}\right)C_g, \tag{8}$$

where  $\mu_0 = 4\pi \times 10^{-7}$  H/m,  $C_g$  = gap capacitance [79].

$$C_g = 0.5hQ_1 \exp\left(-1.86\frac{W_n}{h}\right) \times \left[1 + 4.09\left\{1 - \exp\left(0.75\sqrt{\frac{h}{W_n}}\right)\right\}\right], \tag{9}$$

$$Q_1 = 0.04598\{0.03 + (W_n/h)^{Q_4}\}(0.272 + \epsilon_r 0.07), \tag{10}$$

$$Q_2 = 0.107\left[\frac{W}{h} + 9\right](W_n/h)^{3.23} + 2.09\left(\frac{W_n}{h}\right)^{1.05} + \left[\frac{1.5 + 0.3(W/h)}{1 + 0.6(W/h)}\right], \tag{11}$$

$$Q_3 = \exp(-0.5978) - 0.55, \tag{12}$$

$$Q_4 = 1.23. \tag{13}$$

The impedance of notch loaded patch as shown in Table 11 is given as,

$$Z_{np} = \frac{1}{(1/R) + (1/j\omega L_1) + j\omega C_1}, \tag{14}$$

where

$$L_1 = \Delta L + L, \tag{15}$$

$$C_1 = \frac{C\Delta C}{C + \Delta C}, \tag{16}$$

Figure 8 and S. No. 7 in Table 11 show the modified circuit of antenna after the introduction of notch on the patch with additional coupling impedance  $Z_m$  between two resonator circuits (with notch ( $Z_{np}$ ) and without notch  $Z_{cp}$ ). Impedance  $Z_m$  is in series with mutual inductance  $L_m$  and capacitance  $C_m$  and can be calculated as mentioned in [89]. The equivalent impedance ( $Z_{cp}$ ) of simple rectangular patch ( $L_p \times W_p$ ) antenna without notch is given according to [87].

$$Z_m = j\omega L_m + \frac{1}{j\omega C_m}, \tag{17}$$

where

$$L_m = \frac{k^2(L + L_1) + \sqrt{k^4(L + L_1)^2 + 4k^2(1 - k^2)L L_1}}{2(1 - k^2)}, \tag{18}$$

$$C_m = \frac{-(C + C_1) + \sqrt{(C + C_1)^2 - C C_1(1 - k^2)}}{2}, \tag{19}$$

$$k = \frac{1}{\sqrt{Q_1 Q_2}}, \tag{20}$$

$$Q_1 = R\sqrt{\frac{C}{L}}, \tag{21}$$

$$Q_2 = R\sqrt{\frac{C_1}{L_1}}. \tag{22}$$



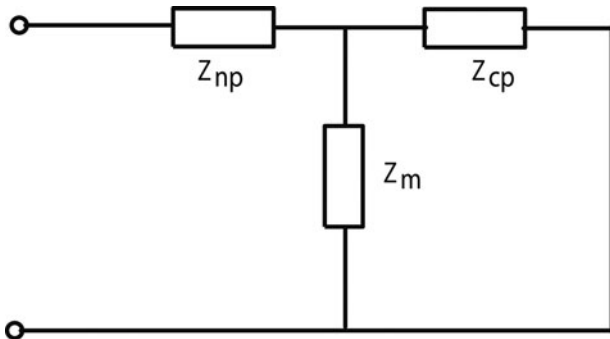


Fig. 8. Equivalent circuit of notch loaded patch antenna.

**Analysis of slot loaded patch**

The slot on the patch (compare S. No. 6 in Table 11) can be analyzed by using the duality relationship between the dipole and slot [82]. Introduction of slot ( $L_s \times W_s$ ) on the patches led to an impedance ( $Z_s = R_r + jX_c$ ) parallel to the input impedance of the antenna as shown in Table 11 at S. No. 6 and is given by equation (23). Further values can be calculated accordingly [91].

$$Z_s = R_r + jX_c, \tag{23}$$

where  $R_r$  and  $X_c$  are given as

$$R_r = 60 \left[ \begin{aligned} &A + I_n(BL_s) - C_i(BL_s) + \frac{1}{2} \sin(BL_s) \{S_i(2BL_s) - 2S_i(BL_s)\} \\ &+ \frac{1}{2} \cos(BL_s) \left\{ A + I_n\left(\frac{BL_s}{2}\right) + C_i(2BL_s) - 2C_i(BL_s) \right\} \end{aligned} \right], \tag{24}$$

$$X_c = 30 \left[ \begin{aligned} &2S_i(BL_s) + \cos(BL_s) \{2S_i(BL_s) - S_i(2BL_s)\} \\ &- \sin(BL_s) \left\{ 2C_i(BL_s) - C_i(2BL_s) - C_i\left(\frac{BW_s^2}{2L_s}\right) \right\} \end{aligned} \right]. \tag{25}$$

$B = 2\pi/\lambda$  is propagation constant in free space and  $S_i$  and  $C_i$  are defined as:

$$S_i(x) = \int_0^x \frac{\sin x}{x} dx, \tag{26}$$

$$C_i(x) = - \int_0^x \frac{\cos x}{x} dx. \tag{27}$$

Hence, the total input impedance of slot loaded antenna can be calculated as:

$$Z_{in} = \frac{Z_s Z_c}{Z_s + Z_c}, \tag{28}$$

where

$$Z_c = Z_{np} + \frac{Z_m Z_{cp}}{Z_m + Z_{cp}}. \tag{29}$$

**Defected ground structure (DGS) and Split ring resonator (SRR)**

The DGS is generally used on ground plane (compare S. No. 8 in Table 11) to improve the antenna radiation but for some antenna structures this technique also helps to improve the antenna bandwidth [89, 96–99]. The DGS structure changes current length path and electrical elements value ( $R1$ ,  $L1$ , and  $C1$ ) of equivalent circuit of microstrip patch antenna. The DGS increases inductance value ( $L1$ ) and reduces capacitance value ( $C1$ ) of resonant circuit (compare S. No. 8 in Table 11). This fact results into large bandwidth ( $f - f_c$ ) ( $f + f_c$ ) of microstrip patch antenna as stated in equation (32). Extremely high impedance bandwidth (112.4%) is reported in [100] as compared to the impedance bandwidth of antennas reported in [2] (54.65%) and [101] (22%). Equivalent circuit model and elemental values of DGS are given below as formulated in [102].

$$R1 = \frac{2Z_o}{\sqrt{(1/|S_{11}|) - (2Z_o(2\pi fC - (1/2\pi fL1))^2 - 1)}, \tag{30}$$

$$L1 = \frac{1}{(2\pi f)^2 C1}, \tag{31}$$

$$C1 = \frac{f_c}{4Z_o \pi (f^2 - f_c^2)}. \tag{32}$$

SRR structure is a very common structure on ground plane (compare S. No. 9 in Table 11) to change the material properties such as permeability and magnetic susceptibility in electric field environment. The SRR structure consists of opposite small gaps in concentric, square, and rectangular nonmagnetic metal-like copper (compare S. No 9 in Table 11). The small opposite gaps behave as two parallel plates and produce a large capacitance value which lowers the resonating frequency. Also, the small structure of SRR results in low radiation losses and very high-quality factor. In antenna design, SRR structure improves the impedance bandwidth as compared to conventional antennas [103–106]. The antenna reported in [106] has a large impedance bandwidth (17.66%) in comparison to the bandwidths of 12% in [103], 6.6/4.8% in [104], and 11.4% in [105]. Equivalent circuit of SRR is depicted in Table 11 (S. No. 9) and its elemental values can be calculated as in [107].

**Fractal geometry**

Initially, the concept of fractal antenna was introduced for the reduction of antenna size. In order to satisfy the demand of bandwidth and compact size of an antenna, researchers are utilizing the fractal geometry in his research to improve the bandwidth for advanced technologies. This antenna increases the effective current length path on the radiating surface after filling the blank space with conducting material. The fractal geometry introduces an additional virtual reactive inductors and capacitors in resonance circuit. This behavior of fractal antenna creates multi-resonance which can be chosen after proper selection of fractal geometry. Number of iterations can increase the radiation property and bandwidth of a fractal antenna.

The fractal antennas [7, 22, 23, 108–112] have been reported at S. No. 10 in Table 11. The antennas reported in [7, 22, 23, 108–112] have utilized the fractal geometry with the introduction of other

reported bandwidth enhancement techniques such as flower shape antenna [7] used fractal geometry with SRR structure, tree shape antennas [22, 23] used notch and DGS, respectively, and the antennas reported in [108–112] used SRR, metamaterial, slot, shorting-pin, and gap coupled structure, respectively. A maximum/minimum bandwidth of 113.13/3.3% in [22, 108] is observed, respectively, among reported antennas at S. No. 10 in Table 11. After comparison of fractal antennas, this is concluded that the fractal geometry can optimize both size and bandwidth provided the introduction of techniques reported in S. No. 1–10 has been used.

### Composite right/left-handed transmission line (CRLH-TL) approach

A miniaturized technique CRLH-TL approach for bandwidth enhancement is presented at S. No. 11 in Table 11. The antennas [113–118] reported at S. No. 11 in Table 11 have utilized the CRLH-TL technique to enhance the bandwidth. The miniaturization of monopole antenna has been achieved by using CRLH-TL unit cells with zeroth-order resonant (ZOR) mode [114]. The ZOR resonance frequency of the antenna does not depend on its length, but it depends on the parameters of CRLH-TL unit cells. Merely ZOR cannot enhance the antenna bandwidth. Therefore, merging of ZOR modes with CRLH-TL unit cell results in an enhancement in bandwidth without decreasing antenna efficiency.

The equivalent circuit model of the basic CRLH-TL unit cell is represented by series combination of inductance  $L_P$  and capacitance  $C_P$  and shunt combination of inductance  $L_Q$  and capacitance  $C_Q$  [113]. In CRLH loading, open circuit and short circuit resonance of ZOR mode is due to the shunt and series branch of inductor and capacitor observed, respectively. The resonance frequencies for the series branches ( $f_o$  (series)) and shunt branch ( $f_o$  (shunt)) can be written as given in [115].

$$f_o \text{ (series)} = \frac{1}{2\pi\sqrt{L_P C_Q}}, \quad (33)$$

$$f_o \text{ (shunt)} = \frac{1}{2\pi\sqrt{L_Q C_P}}. \quad (34)$$

The antennas reported in [113, 114] have utilized the CRLH-TL two-unit cell with a bandwidth of 160% between 1.55 and 14.25 GHz for UWB applications and the antennas reported in [115, 116] with four-unit cell have been designed with a maximum bandwidth of 173% between 1.0 and 13.6 GHz. However, two-unit cells of same size for triple band (bandwidth of 200, 500, and 600 MHz) and three-unit cell of different sizes for quad band (bandwidth more than 100 MHz for each band) applications have been reported [115, 116]. The antenna [117] utilizes the CPW and stub for circular polarization (impedance bandwidth of 1770 MHz between 3.78 and 5.55 GHz and ARBW of 1750 MHz between 3.50 and 5.25 GHz) and band notch with slit loaded (impedance bandwidth of 2200 MHz between 3.28 and 5.48 GHz with a band notch from 4.18 to 4.65 GHz). The antenna [118] has been designed with CRLH-TL approach and gap coupled concept results dual-band characteristic at 4.84 and 5.22 GHz resonance with the impedance bandwidth of 100 and 50 MHz, respectively.

### Conclusions

A comprehensive review of microstrip patch antenna concerning flower shape, leaf shape, tree shape, fan shape, Pi shape, butterfly

shape, and bat shape antennas along with bandwidth enhancement techniques has been carried out. The antenna size, dielectric materials, resonating band, peak gain, radiation efficiency, simulating tools, and their applications have been carefully investigated.

From the discussions carried out in this review paper, the following points can be highlighted:

- (1) Most of the reported antenna designs are simulated through the HFSS based on finite element method (FEM) algorithm and validated well with experimental results. IE3D (MoM-based program) performs simulation inherently faster (minimum time is required per iteration) while HFSS (FEM-based program) is inherently able to analyze much more general geometry of antenna. Ansoft HFSS provides very neat and adaptive mesh refinement while CST allows better handling of difficult electromagnetic coupling between its different parts. FEM and finite integration technique (FIT)-based program are more suitable than other simulation package for modern small and compact size of antenna.
- (2) The leaf shape antenna [13] exhibits extremely wideband impedance bandwidth (28.4 GHz) covering L, C, X, and Ku bands of electromagnetic spectrum. The bandwidth (28.4 GHz) of leaf shape antenna [13] is larger than the antennas reported in [5–12, 14–41] of Tables 1–5. The simulated peak gain of 18.4 dBi of tree shape antenna [24] and measured peak gain of 9.72 dBi of bat shape antenna [40] are larger than the gain reported in [5–23, 25–38].
- (3) Antenna size of reported works is in millimeter scale. The antenna reported in [7] has a very small antenna dimensions (144 mm<sup>2</sup>) whereas the antenna reported in [24] and [37] has very large antenna dimensions 22 500 and 90 000 mm<sup>2</sup>, respectively, as compared to the antennas reported in Tables 1–10. The compact antenna [7] has been designed for IEEE802.11, GSM, WLAN, and WiMAX applications. Among several dielectric materials such as FR4 epoxy, RT/Duroid, Foam, Air, Teflon, and Nylon, the FR4 epoxy is mostly used to design microstrip antenna due to its wide availability and feasible cost.

Owing to the review of different antenna geometry (compare Tables 1–10) specially flower shape, leaf shape, tree shape, fan shape, Pi shape, butterfly shape, bat shape, wearable, multiband, monopole, fractal, and CRLH-TL antennas, it is concluded that the shapes are notched on the edges of radiating patch to enhance the perimeter as well as impedance bandwidth of the antenna.

This argument is in conformity with the fact of a maximum current distribution appears on the edges rather than the center of the radiating patch.

After examining the wearable antennas reported in Table 8, it is concluded that the wearable antenna plays a very vital role in medical applications but following issues are yet to be improved: to reduce the bending effect, make it washable, reduce electromagnetic interference in human body.

- (4) A critical review of bandwidth enhancement techniques and equivalent circuit model of microstrip patch antenna is presented in Table 11. The circuit theory model concept is merely taken into consideration for the review of bandwidth enhancement techniques. From the above discussion, it can be clearly concluded that the shorting wall, shorting pin, and loading of slot are various types of inductive loading

whereas the notch, DGS, gap coupled, SRR, and CRLH-TL are several types of inductive as well as capacitive loading. The resonance behavior of microstrip patch antenna depends on the overall input impedance of the patch antenna and the input impedance of antenna can be changed by any physical change in antenna structure with the help of reported techniques listed in Table 11.

**Acknowledgements.** We would like to show our gratitude to Nidhi Singh for her support in language editing that greatly improved the manuscript.

## References

- Kumar G and Ray KP (2003) *Broadband Microstrip Antenna*. Norwood, MA: Artech House.
- Mishra B, Singh V, Singh RK, Singh N and Singh R (2018) A compact UWB patch antenna with defected ground for Ku/K band applications. *Microwave and Optical Technology Letters* **60**, 1–6.
- Singh V, Mishra B, Narayan Tripathi P and Singh R (2016) A compact quad-band microstrip antenna for S and C-band applications. *Microwave and Optical Technology Letters* **58**, 1365–1369.
- Mishra B (2019) An ultra compact triple band antenna for X/Ku/K band applications. *Microwave and Optical Technology Letters* **61**, 1857–1862.
- Patre SR and Singh SP (2015) CPW-fed flower-shaped patch antenna for broadband applications. *Microwave and Optical Technology Letters* **57**, 2908–2913.
- Rani Patre S and Singh SP (2016) Study of microstrip line-fed flower-shaped patch antenna providing enhanced bandwidth and radiation efficiency. *Microwave and Optical Technology Letters* **58**, 2041–2046.
- Elavarasi C and Shanmuganatham T (2017) SRR loaded CPW-fed multiple band rose flower-shaped fractal antenna. *Microwave and Optical Technology Letters* **59**, 1720–1724.
- Kim D-J, Choi J-H and Kim Y-S (2013) CPW-fed ultrawideband flower-shaped circular fractal antenna. *Microwave and Optical Technology Letters* **55**, 1792–1795.
- Tang M-C, Ziolkowski RW and Xiao S (2014) Compact wideband printed flower slot antenna. *Microwave and Optical Technology Letters* **56**, 1465–1468.
- Ooi BL and Ang I (2005) Broadband semicircle-fed flower-shaped microstrip patch antenna. *Electronics Letters* **41**, 939.
- Soorya R and Ramprakash K. UWB microstrip patch antenna with flower shaped patch and cavity structure. 2016 International Conference on Wireless Communication, Signal Processing and Networking, IEEE; 2016, p. 2080–2084. doi:10.1109/WiSPNET.2016.7566508
- Ahmed OMH and Sebak AR (2009) A novel maple-leaf shaped UWB antenna with a 5.0–6.0 GHz band-notch characteristic. *Progress in Electromagnetics Research C* **11**, 39–49.
- Bai X-F, Zhong S-S and Liang X-L (2006) Leaf-shaped monopole antenna with extremely wide bandwidth. *Microwave and Optical Technology Letters* **48**, 1247–1250.
- Ozkaya U and Seyfi L (2016) A comparative study on parameters of leaf-shaped patch antenna using hybrid artificial intelligence network models. *Neural Computing and Applications* **29**, 35–45.
- Ahdi Rezaeieh S and Kartal M (2012) Miniaturized leaf-shaped monopole antenna with filtering properties. *Microwave and Optical Technology Letters* **54**, 2638–2642.
- Lotfi Neyestanak AA (2008) Ultra wideband rose leaf microstrip patch antenna. *Progress in Electromagnetics Research* **86**, 155–168.
- Singh V, Mishra B, Pandey AK, Patel AK, Yadav S and Singh R (2017) Triple band CPW fed monopole leaf shaped patch antenna. *International Journal on Communications Antenna and Propagation* **7**, 135.1–7.
- Zeng X, Zhang C, Wang Y and Xie C. A novel planar tree-shaped fractal dipole patch antenna. 2010 International Conference on Microwave and Millimeter Wave Technology, IEEE; 2010: 359–361. doi:10.1109/ICMMT.2010.5524965
- Kumar D, Kumar A and Singh AK. Design analysis of Pythagoras tree shaped multiband fractal antenna. 2014 International Conference on Computational Intelligence and Communication Networks, IEEE; 2014: 41–45. doi:10.1109/CICN.2014.21
- Arun V and Karl Marx LR (2017) Micro-controlled tree shaped reconfigurable patch antenna with RF-energy harvesting. *Wireless Personal Communications* **94**, 2769–2781.
- Mishra G and Sahu S (2016) Nature inspired tree shaped antenna with dual band notch for UWB applications. *Microwave and Optical Technology Letters* **58**, 1658–1661.
- Singhal S, Goel T and Singh AK (2015) Inner tapered tree-shaped fractal antenna for UWB applications. *Microwave and Optical Technology Letters* **57**, 559–567.
- Park JK, An HS and Lee JN (2008) Design of the tree-shaped UWB antenna using fractal concept. *Microwave and Optical Technology Letters* **50**, 144–150.
- Shen H, Huang K and Dong L (2012) A high gain tree-shaped array antenna designed by competitive algorithm of simulating natural tree growth. *International Journal of RF and Microwave Computer-Aided Engineering* **22**, 669–674.
- Mathew S, Anitha R, Roshna TK, Nijas CM, Aanandan CK, Mohanan P and Vasudevan K (2014) A fan-shaped circularly polarized patch antenna for UMTS band. *Progress in Electromagnetics Research C* **52**, 101–107.
- Babakhani B and Sharma SK. Wideband circularly polarized fan-shaped antenna on a HIS structure. 2016 IEEE International Symposium on Antennas and Propagation, IEEE; 2016: 125–126. doi:10.1109/APS.2016.7695771
- Liu X, Kong Y, Li Y and Yu K. A fan-shaped band-notched UWB antenna using combined filtering techniques. 2016 IEEE/ACES International Conference on Wireless Information Technology and Systems and Applied Computational Electromagnetics, IEEE; 2016, p. 1–2. doi:10.1109/ROPACES.2016.7465395
- Ojaroudi N, Mehranpour M and Ghadimi N (2014) Fan-shaped antenna with triband-notched characteristic for UWB applications. *Microwave and Optical Technology Letters* **56**, 2426–2430.
- Wang C, Yan Z-H, Li B and Li S (2012) An ultra-wideband CPW-fed monopole antenna with fan-shaped structure. *Microwave and Optical Technology Letters* **54**, 2878–2880.
- Hiraguri K, Koshiji F and Koshiji K. A wideband antenna with fan-shaped and trapezoidal elements on printed circuit board for ultra wide-band radio. 2013 IEEE 2nd Global Conference on Consumer Electronics, IEEE; 2013: 267–268. doi:10.1109/GCCE.2013.6664820
- Kumar S and Vishwakarma DK (2016) Compact fan shaped circularly polarized microstrip patch antenna. *Microwave and Optical Technology Letters* **58**, 882–886.
- Choi S-H, Kwak D, Lee H-C and Kwak K-S (2010) Design of a dual-band  $\pi$ -shaped microstrip patch antenna with a shorting pin for 5.2/5.8 GHz WLAN systems. *Microwave and Optical Technology Letters* **52**, 825–827.
- Chen H-M (2001) Single-feed dual-frequency rectangular microstrip antenna with  $\pi$ -shaped slot. *IEE Proceedings - Microwaves, Antennas and Propagation* **148**, 60.
- Arora M, Sharma A and Ray K (2014) A  $\Pi$ -slot microstrip antenna with band rejection characteristics for ultra wideband applications. *Advances in Intelligent Systems and Computing*, 1135–1144. doi: 10.1007/978-81-322-1602-5\_119
- Deshmukh AA, Nishad A, Gosavi G, Narayanan P, Nayak S and Ambekar AG. Novel  $\pi$ -shape microstrip antenna design for multi-band response,” Proceedings of International Conference on Wireless Communication. Lecture Notes on Data Engineering and Communications Technologies, 2018;185–193.
- Sun L, He M, Hu J, Zhu Y and Chen H (2015) A butterfly-shaped wide-band microstrip patch antenna for wireless communication. *International Journal of Antennas and Propagation* **2015**, 1–8.
- Ye Q, Ning Chen Z and See TSP (2009) A novel butterfly-shaped monopole UWB antenna. *Microwave and Optical Technology Letters* **51**, 590–593.
- Tiwari RN, Singh P and Kanaujia BK (2017) Butterfly shape compact microstrip antenna for wideband applications. *Progress in Electromagnetics Research Letters* **69**, 45–50.

39. Fakharian MM, Rezaei P and Azadi A (2015) A planar UWB bat-shaped monopole antenna with dual band-notched for WiMAX/WLAN/DSRC. *Wireless Personal Communications* **81**, 881–891.
40. Kuralay EN, Uzun EF and Imeci T. Bat shaped patch antenna at 14.6 GHz. 2016 IEEE/ACES International Conference on Wireless Information Technology and Systems and Applied Computational Electromagnetics, IEEE; 2016: 1–2. doi:10.1109/ROPACES.2016.7465456
41. Mirmosaei SS, Afjei SE, Mehrshahi E and Fakharian MM (2016) A dual band-notched ultra-wideband monopole antenna with spiral-slots and folded SIR-DGS as notch band structures. *International Journal of Microwave and Wireless Technologies* **8**, 1197–1206.
42. Singh N, Singh AK and Singh VK (2015) Design and performance of wearable ultra-wide band textile antenna for medical applications. *Microwave and Optical Technology Letters* **57**, 1553–1557. doi: 10.1002/mop.29131
43. Singh VK, Dhupkariya S and Bangari N (2017) Wearable ultra-wide dual band flexible textile antenna for WiMax/WLAN application. *Wireless Personal Communications* **95**, 1075–1086.
44. Yadav A, Singh VK and Mohan H (2019) Design of a U-shaped circularly polarized wearable antenna with DGS on a fabric substrate for WLAN and C-band applications. *Journal of Computational Electronics* **18**, 1103–1109.
45. Yadav A, Singh VK, Yadav P, Beliya AK, Bhoi AK and Barsocchi P (2020) Design of circularly polarized triple-band wearable textile antenna with safe low SAR for human health. *Electronics* **9**, 1–17.
46. Yadav A, Singh VK, Bhoi AK, Marques G, Zapirain BG and Díez IT (2020) Wireless body area networks: UWB wearable textile antenna for telemedicine and mobile health systems. *Micromachines* **11**, 1–22.
47. Sudeep B, Goswami AK and Yadav MV (2019) Miniaturized dual-band antenna with a rectangular patch and symmetrically placed circles in the partial ground plane. *Progress in Electromagnetics Research M* **78**, 29–37.
48. Verma RK and Srivastava DK (2020) Design and analysis of triple-band rectangular microstrip antenna loaded with notches and slots for wireless applications. *Wireless Personal Communications* **114**, 1847–1864.
49. Kaur A, Singh G and Kaur M (2017) Miniaturized multiband slotted microstrip antenna for wireless applications. *Wireless Personal Communications* **96**, 441–453.
50. Gangwar AK and Alam MS (2019) A miniaturized quad-band antenna with slotted patch for WiMAX/WLAN/GSM applications. *AEU-International Journal of Electronics and Communications* **112**, 152911, 1–9.
51. Ali T, Prasad KD and Biradar RC (2018) A miniaturized slotted multi-band antenna for wireless applications. *Journal of Computational Electronics* **17**, 1056–1070.
52. Singh V, Mishra B, Dwivedi AK and Singh R (2018) Inverted L-notch loaded hexa band circular patch antenna for X, ku/K band applications. *Microwave and Optical Technology Letters* **60**, 2081–2088.
53. Sachan R and Dhubkaryia DC (2021) Photonic bandgap hepta-band stacked microstrip antenna for L, S and C band applications. *Wireless Personal Communications* **116**, 1913–1931.
54. Luk KM, Mak CL, Chow YL and Lee KF (1998) Broadband microstrip patch antenna. *Electronics Letters* **34**, 1442–1443.
55. Mishra B, Singh V and Singh R (2017) Dual and wide-band slot loaded stacked microstrip patch antenna for WLAN/WiMAX applications. *Microsystem Technologies* **23**, 3467–3475.
56. Ooi B-L, Qin S and Leong M-S (2002) Novel design of broad-band stacked patch antenna. *IEEE Transactions on Antennas and Propagation* **50**, 1391–1395.
57. Shi W, Qian Z and Ni W (2016) Dual-band stacked annular slot/patch antenna for omnidirectional radiation. *IEEE Antennas and Wireless Propagation Letters* **15**, 390–393.
58. Qian K and Tang XH (2011) Compact LTCC dual-band circularly polarized perturbed hexagonal microstrip antenna. *IEEE Antennas and Wireless Propagation Letters* **10**, 1212–1215.
59. Nayeri P, Lee K-F, Elsherbeni AZ and Yang F (2011) Dual-band circularly polarized antennas using stacked patches with asymmetric U-slots. *IEEE Antennas and Wireless Propagation Letters* **10**, 492–495.
60. Kumar G and Gupta K (1985) Nonradiating edges and four edges gap-coupled multiple resonator broad-band microstrip antennas. *IEEE Transactions on Antennas and Propagation* **33**, 173–178.
61. Ray KP, Sevani V and Kakatkar S (2006) Compact broadband gap-coupled rectangular microstrip antennas. *Microwave and Optical Technology Letters* **48**, 2384–2389.
62. Meshram MK and Vishvakarma BR (2001) Gap-coupled microstrip array antenna for wide-band operation. *International Journal of Electronics* **88**, 1161–1175.
63. Guha D and Antar YM (2006) Circular microstrip patch loaded with balanced shorting pins for improved bandwidth. *Antennas and Wireless Propagation Letters* **5**, 217–219.
64. Waterhouse RB, Targonski SD and Kokotoff DM (1998) Design and performance of small printed antennas. *IEEE Transactions on Antennas and Propagation* **46**, 1629–1633.
65. Malekpoor H and Jam S (2013) Enhanced bandwidth of shorted patch antennas using folded-patch techniques. *IEEE Antennas and Wireless Propagation Letters* **12**, 198–201.
66. Yoon C, Choi S-H, Lee H-C and Park H-D (2008) Small microstrip patch antennas with short-pin using a dual-band operation. *Microwave and Optical Technology Letters* **50**, 367–371.
67. Malekpoor H and Jam S (2013) Design of an ultra-wideband microstrip patch antenna suspended by shorting pins. *Wireless Personal Communications* **71**, 3059–3068.
68. Li Y, Chair R, Luk KM and Lee KF (2004) Broadband triangular patch antenna with a folded shorting wall. *IEEE Antennas and Wireless Propagation Letters* **3**, 189–192.
69. Mak CL, Chair R, Lee KF, Luk KM and Kishk AA (2003) Half U-slot patch antenna with shorting wall. *Electronics Letters* **39**, 1779.
70. Han T and Sim C (2009) Shorted planar triangular patch antenna with dual-frequency operation. *AEU – International Journal of Electronics and Communications* **63**, 103–107.
71. Chiu CY, Wong H and Chan CH (2007) Study of small wideband folded-patch-feed antennas. *IET Microwaves, Antennas and Propagation* **1**, 501.
72. Ansari JA, Singh P, Dubey SK, Khan RU and Vishvakarma BR (2009) Analysis of stacked V-slot loaded patch antenna for wideband application. *Microwave and Optical Technology Letters* **51**, 324–330.
73. Jan J-Y and Su J-W (2005) Bandwidth enhancement of a printed wide-slot antenna with a rotated slot. *IEEE Transactions on Antennas and Propagation* **53**, 2111–2114.
74. James JR and Hall PS (1989) *Handbook of Microstrip Antennas*. London, UK: Peter Peregrinus Ltd.
75. Kamakshi K, Singh A, Ansari JA and Mishra A (2013) Analysis of dual inverted C-slot patch antenna for limited space applications. *Proceedings of the National Academy of Sciences, India Section A: Physical Sciences* **83**, 175–180.
76. Jackson D and Alexopoulos N (1985) Gain enhancement methods for printed circuit antennas. *IEEE Transactions on Antennas and Propagation* **33**, 976–987.
77. Yang H and Alexopoulos N (1987) Gain enhancement methods for printed circuit antennas through multiple superstrates. *IEEE Transactions on Antennas and Propagation* **35**, 860–863.
78. Majid HA, Rahim MKA and Masri T (2009) Microstrip antenna's gain enhancement using left-handed metamaterial structure. *Progress in Electromagnetics Research M* **8**, 235–247.
79. Yang H-YD, Alexopoulos NG and Yablonovitch E (1997) Photonic band-gap materials for high-gain printed circuit antennas. *IEEE Transactions on Antennas and Propagation* **45**, 185–187.
80. Boutayeb H and Denidni TA (2007) Gain enhancement of a microstrip patch antenna using a cylindrical electromagnetic crystal substrate. *IEEE Transactions on Antennas and Propagation* **55**, 3140–3145.
81. Kuo J-S and Hsieh G-B (2003) Gain enhancement of a circularly polarized equilateral-triangular microstrip antenna with a slotted ground plane. *IEEE Transactions on Antennas and Propagation* **51**, 1652–1656.
82. Xing Z, Wang L, Li J and Wei K (2014) Radiation efficiency improvement method for multifeed circular polarization antenna array with mutual coupling effect. *International Journal of Antennas and Propagation* **2014**, 1–10.

83. Li L, Zhang Y, Wang J, Zhao W, Liu S and Xu R (2014) Bandwidth and gain enhancement of patch antenna with stacked parasitic strips based on LTCC technology. *International Journal of Antennas and Propagation* **2014**, 1–5.
84. Whittow WG and Motevasselian A (2015) Patch size reduction of rectangular microstrip antennas by means of a cuboid ridge. *IET Microwaves, Antennas and Propagation* **9**, 1727–1732.
85. Chen W-S, Wu C-K and Wong K-L (2001) Novel compact circularly polarized square microstrip antenna. *IEEE Transactions on Antennas and Propagation* **49**, 340–342.
86. Balanis CA (2005) *Antenna Theory*, 3rd Edn. NY, USA: Wiley-Interscience New York.
87. Singh V, Mishra B and Singh R (2019) Anchor shape gap coupled patch antenna for WiMAX and WLAN applications. *COMPEL – International Journal for Computation and Mathematics in Electrical and Electronic Engineering* **38**, 263–286.
88. Mishra A, Ansari JA, Kamakshi K, Singh A, Aneesh M and Vishvakarma BR (2015) Compact dualband rectangular microstrip patch antenna for 2.4/5.12-GHz wireless applications. *Wireless Networks* **21**, 347–355.
89. Shivnarayan and Vishvakarma BR (2006) Analysis of notch-loaded patch for dual-band operation. *Indian Journal of Radio & Space Physics* **35**, 435–442.
90. Tsai H-S and York RA (1996) FDTD analysis of CPW-fed folded-slot and multiple-slot antennas on thin substrates. *IEEE Transactions on Antennas and Propagation* **44**, 217–226.
91. Singh A, Aneesh M, Kamakshi K and Ansari JA (2018) Circuit theory analysis of aperture coupled patch antenna for wireless communication. *Radioelectronics and Communication Systems* **61**, 168–179.
92. Ansari JA, Singh P, Yadav NP and Vishvakarma BR (2009) Analysis of shorting PIN loaded half disk patch antenna for wideband operation. *Progress in Electromagnetics Research C* **6**, 179–192.
93. Mishra B, Singh V and Singh R (2018) Gap coupled dual-band petal shape patch antenna for WLAN/WiMAX applications. *Advances in Electrical and Electronic Engineering* **16**, 185–198.
94. Ansari JA, Yadav NP, Mishra A, Singh P and Vishvakarma BR (2012) Analysis of multilayer rectangular patch antenna for broadband operation. *Wireless Personal Communications* **62**, 315–327.
95. Mishra A, Singh P, Yadav NP, Ansari JA and Vishvakarma BR (2009) Compact shorted microstrip patch antenna for dual band operation. *Progress in Electromagnetics Research C* **9**, 171–182.
96. Singh A, Ansari JA, Kamakshi K, Mishra A and Aneesh M (2014) Compact notch loaded half disk patch antenna for dualband operation. *Annals of Telecommunications – Ann Des Télécommunications* **69**, 475–483.
97. Shivnarayan and Vishvakarma BR (2005) Analysis of dual-band patch antenna for mobile communications. *Microwave and Optical Technology Letters* **47**, 558–564.
98. Ansari JA, Singh P, Dubey SK, Khan RU and Vishvakarma BR (2009) Analysis of symmetrically notch loaded stacked disk patch antenna for wideband application. *Microwave and Optical Technology Letters* **51**, 653–659.
99. Shackelford AK, Leong S-Y and Lee K-F Simulation of a probe-fed notched patch antenna with a shorting post. *IEEE Antennas and Propagation Society International Symposium 2001 Digest Held conjunction with USN National Radio Science Meeting (Cat. No.01CH37229)*, vol. 2, IEEE; n.d., p. 708–11. doi:10.1109/APS.2001.959822.
100. Chiang KH and Tam KW (2008) Microstrip monopole antenna with enhanced bandwidth using defected ground structure. *IEEE Antennas and Wireless Propagation Letters* **7**, 532–535.
101. Guha D and Kumar C (2014) Defected ground structure (DGS)-integrated rectangular microstrip patch for improved polarisation purity with wide impedance bandwidth. *IET Microwaves, Antennas and Propagation* **8**, 589–596.
102. Khandelwal MK, Kanaujia BK and Kumar S (2017) Defected ground structure: fundamentals, analysis, and applications in modern wireless trends. *International Journal of Antennas and Propagation* **2017**, 1–22.
103. Arora C, Pattnaik SS and Baral RN (2018) Bandwidth enhancement of microstrip patch antenna array using spiral split ring resonator. *Information Systems Design and Intelligent Applications. Advances in Intelligent Systems and Computing* **672**, 435–441.
104. da Silva JL, de Andrade HD, Fernandes HCC, da Silva IBT, Júnior IDSQ, Pereira JPP and Neto ASS (2015) Microstrip patch antenna project with split ring resonator periodically arrayed on the substrate. *Microwave and Optical Technology Letters* **57**, 2715–2720.
105. Patel SK, Argyropoulos C and Kosta YP (2017) Broadband compact microstrip patch antenna design loaded by multiple split ring resonator superstrate and substrate. *Waves in Random and Complex Media* **27**, 92–102.
106. da Silva IBT, de Andrade HD, da Silva JL, Fernandes HCC and Pereira JPP (2015) Design of microstrip patch antenna with complementary split ring resonator device for wideband systems application. *Microwave and Optical Technology Letters* **57**, 1326–1330.
107. Baena JD, Bonache J, Martin F, Sillero RM, Falcone F, Lopetegi T, Laso AG, Garcia JG, Gil I, Portillo MF, and Sorolla M (2005) Equivalent-circuit models for split-ring resonators and complementary split-ring resonators coupled to planar transmission lines. *IEEE Transactions on Microwave Theory and Techniques* **53**, 1451–1461.
108. Sharma V, Lakwar N, Kumar N and Garg T (2018) Multiband low-cost fractal antenna based on parasitic split ring resonators. *IET Microwaves, Antennas & Propagation* **12**, 913–919.
109. Gupta N, Saxena J and Bhatia KS (2020) Optimized metamaterial-loaded fractal antenna using modified hybrid BF-PSO algorithm. *Neural Computing & Applications* **32**, 7153–7169.
110. Ali T, Saadh AWM and Biradar RC (2018) A fractal quad-band antenna loaded with L-shaped slot and metamaterial for wireless applications. *International Journal of Microwave and Wireless Technologies* **10**, 826–834.
111. Souza EAM, Oliveira PS, Dassuncao AG, Mendonca LM and Peixeiro C (2019) Miniaturization of a microstrip patch antenna with a Koch fractal contour using a social spider algorithm to optimize shorting post position and inset feeding. *International Journal of Antennas and Propagation* **2019**, 1–10. doi: 10.1155/2019/6284830.
112. Srivastava DK, Khanna A and Saini JP (2016) Design of a wideband gap-coupled modified square fractal antenna. *Journal of Computational Electronics* **15**, 239–247.
113. Rajasekhar NV and Kumar DS (2016) A miniaturized UWB via-less CRLH-TL loaded CPW FED patch antenna. *Microwave and Optical Technology Letters* **58**, 2485–2492.
114. Nuthakki VR and Dhamodharan S (2017) Via-less CRLH-TL unit cells loaded compact and bandwidth-enhanced metamaterial based antennas. *AEU-International Journal of Electronics and Communications* **80**, 48–58.
115. Abdalla M, Hu Z and Muvianto C (2017) Analysis and design of a triple band metamaterial simplified CRLH cells loaded monopole antenna. *International Journal of Microwave and Wireless Technologies* **9**, 903–913.
116. Abdalla M and Hu Z (2018) Design and analysis of a compact quad band loaded monopole antenna with independent resonators. *International Journal of Microwave and Wireless Technologies* **10**, 479–486.
117. Ghosh K and Das S (2020) Circularly polarized ACPW fed CRLH-TL based ZOR antenna with band notch characteristics. *International Journal of Microwave and Wireless Technologies* **12**, 387–397.
118. Ahmed Z, Ahmed MM, Ihsan MB, Chaudhary AA and Arif JK (2019) Novel dual band patch antenna with gap coupled composite right/left-handed transmission line. *International Journal of Microwave and Wireless Technologies* **11**, 87–93.



**Brijesh Mishra** received his M. Tech. (Electronics Engineering) and D.Phil. (RF and Microwaves) degrees from the University of Allahabad in 2012 and 2018. Dr. Brijesh Mishra worked as an Assistant Professor in the Department of Electronics and Communication Engineering at Shambhunath Institute of Engineering and Technology (SIET) during 2012–2013 and 2017–2018. Presently, he is working as an Assistant Professor (NPIU-MHRD) in the Department of Electronics and Communication Engineering at Madan Mohan Malaviya University of Technology. He has published more than 38 research papers in journals of international repute, international conferences, and books chapters and he

has also edited an international book entitled “VLSI, Microwave and Wireless Technologies-Proceedings of ICMWT 2021”. Dr. Brijesh Mishra is the principal investigator and co-investigator in two NPIU and World Bank funded projects. He is the recipient of awards like Excellence in Performance and Outstanding contributions. He has served as Organising Track Chair and Organising Secretary in IEEE Conference (ICE3-2020) and Springer Conference (ICVMWT-2021), respectively. He is a member of IEEE, ISTE, IE(I), IETE, IAENG, and IFERP. His research interest includes modeling, simulation, and fabrication of RF and microwave devices and its applications.



**Ramesh Kumar Verma** received his M. Tech degree in year 2015 from Bundelkhand Institute of Engineering and Technology Jhansi, in Digital communication. He had completed B. Tech in year 2009 from Raj Kumar Goel Institute of Technology Ghaziabad in Electronics and Communication Engineering. He is currently pursuing Ph.D. from AKTU Lucknow, Uttar Pradesh, India. He is an expert

in antenna designing, fabrication, IE3D simulation software and Particle Swarm Optimization (PSO) Algorithm. Presently, he is working on optimization of microstrip patch antenna with PSO and curve fitting.



**Yashwanth N** is working as an Associate Professor in the Department of Electronics and Communication Engineering, Nagarjuna College of Engineering & Technology, Bengaluru, India. He has completed his Ph.D. from Visvesvaraya Technological University, Belagavi in 2020. In 2012, he received his M. Tech degree in Signal Processing and VLSI from Jain University, Bengaluru. He completed his B.E. in

Electronics and Communication Engineering from Visvesvaraya Technological University, Belagavi in 2010. He has worked as an Assistant Professor at Rajeev

Institute of Technology, Hassan, with 8 years of teaching experience to UG and PG students. He has authored or co-authored more than 15 research papers in international journal/conference proceedings. His research interests include wireless sensor networks, signal processing, VLSI, communication systems, and antennas. He is a reviewer of many international journal/conference proceedings.



**Rakesh Kumar Singh** received his M. Tech (Electronics Engineering) and Ph.D. (Electronics and Communication) degrees from Sam Higginbottom University of Agriculture, Technology and Sciences during 2013 and 2018, respectively. He has completed his B.Sc. and M.Sc. degrees from the University of Allahabad in 1999 and 2003, respectively. Currently, he is working as a Director at SIET, Prayagraj Uttar

Pradesh, affiliated from AKTU. He has teaching and research experience of about 16 years. Dr. Rakesh Kumar Singh has published more than 14 papers in International Journals and Conferences and supervised more than three M. Tech thesis. His research interest includes modeling and simulation of VLSI devices, RF and microwave devices, and its applications.